Department of Mechanical and Aerospace Engineering

FUNDAMENTAL INVESTIGATIONS OF THE FINITE ELEMENT SOLUTIONS FOR ACOUSTIC PROPAGATION IN DUCTS

N. J. Walkington, T. W. Wicks and N. Eversman
University of Missouri-Rolla
Rolla, Missouri 65401

FINAL REPORT
NASA LANGLEY NAG-1-198

University of Missouri-Rolla

FUNDAMENTAL INVESTIGATIONS OF THE FINITE ELEMENT SOLUTIONS FOR ACOUSTIC PROPAGATION IN DUCTS

N. J. Walkington*, T. M. Wicks† and W. Eversman*
University of Missouri-Rolla
Rolla, Missouri 65401

FINAL REPORT

NASA LANGLEY NAG-1-198

*Department of Mechanical Engineering
†Department of Engineering Mechanics

ABSTRACT

The question of convergence of three finite element algorithms for the modelling of acoustic transmission in ducts carrying a nonuniform mean flow is addressed. The details of each algorithm are stated and example calculations in uniform and nonuniform ducts are made and assessed for accuracy and convergence.

The algorithm based on the assumption of irrotationality is found to be highly convergent. This algorithm is the one used in current turbo-fan inlet acoustic radiation codes. A theoretical analysis indicating convergence is supported by example calculations.

Two additional algorithms which do not require irrotationality are found to be less convergent, and perhaps not convergent at all for certain severely sheared velocity profiles. No theoretical convergence criteria can presently be established for these algorithms and convergence difficulties are shown here by example. Included in this class of algorithms is the duct analysis program ADAM which is known to display apparently non-convergent solutions in certain cases.

I. INTRODUCTION

It has become apparent that the several finite element approximations used in the modelling of acoustic propagation in nonuniform ducts do not possess consistent convergence characteristics. In particular, experience with approximations based on an assumption of irrotational mean flow and acoustic perturbation indicates that, at least over the fairly broad parametric range so far investigated, convergence characteristics are good. On the other hand, when the irrotational assumption is not imposed, necessitating a finite element approximation based on the primitive form of the acoustic equations (in terms of pressure and two or three velocity components), serious convergence problems can occur, particularly when the mean flow has steep gradients, representative of typical boundary layers. It is the purpose of this study to attempt to isolate with simple examples the nature of the difference in convergence characteristics of the finite element algorithms.

In modelling acoustic propagation in ducts the following assumptions are often made:

1. The fluid is an inviscid ideal gas.
2. The linearized equations of motion accurately describe the propagation of the acoustic disturbances.
3. The motion of the fluid is irrotational.

For the aircraft engine inlet problem assumptions 1 and 2 imply assumption 3 since, for this problem, the fluid is initially irrotational. By the Helmholtz Vorticity Theorem, the fluid remains irrotational. However, it is known that near surfaces assumption 1 breaks down, since the effects of the fluid viscosity are then significant. In order to compensate for this deviation, without giving up too many of the simplifications afforded by assumptions 1-3 the following could be assumed:

4. The motion of small disturbances is well described by the linearized inviscid equations with a viscous mean flow substituted in place of the inviscid mean flow. In other words, the coefficients of the linear equations are altered to represent a viscous mean flow.

Assumption 4 has no physical, mathematical or intuitive justification, and for this reason it is generally argued that it is not appropriate. However, we do make some calculations with it here to demonstrate convergence.

Several numerical algorithms have been developed to model the duct acoustics problem, [1-14], probably the most versatile of which are the finite element methods (FEM's). However, it has been reported [7] that in certain instances some algorithms do not converge. In this document, we consider three finite element algorithms used to model duct acoustics problems; one based on a velocity potential formulation and the other two based upon the primitive equations. It is shown that the algorithm using the velocity potential will converge for a very broad class of mean flows and geometries. The other two algorithms are not ammenable to such analysis, so numerical experiments were conducted in order to estimate what problems may be solved with these algorithms and to compare the algorithms.

Fix, Nicolaides, and Gunzburger [11-13] consider a least squares algorithm to solve the acoustics problem using the primitive equations. They prove that for the no flow case their algorithm will converge optimally when a special class of finite element grids is used. A similar least squares algorithm was proposed by Astley and Eversman [3]. However, they reported that better results were obtained with a classical Galerkin type approximation.

II. ACOUSTIC EQUATIONS AND BOUNDARY CONDITIONS

In this section we consider the acoustic equations and boundary conditions for a duct, Ω.

Assumptions 1 and 2, or 4 lead to the following equations for the acoustic velocity and pressure in Ω.

$$\frac{i\omega}{c^2} p + \underset{\sim}{\nabla}.(\rho \underset{\sim}{u} + \frac{1}{c^2} p \underset{\sim}{U}) = 0$$

$$i\omega \underset{\sim}{u} + (\underset{\sim}{U}.\nabla)\underset{\sim}{u} + (\underset{\sim}{u}.\nabla)\underset{\sim}{U} + \underset{\sim}{\nabla}(\frac{p}{\rho}) = 0 \qquad (2.1)$$

where

$p, \underset{\sim}{u}$ are the acoustic pressure and velocity

$\rho, c, \underset{\sim}{U}$ are the mean flow density, speed of sound and velocity, respectively.

ω is the frequency.

If assumption 1 is used the mean flow $(\rho, c, \underset{\sim}{U})$ should satisfy

$$\underset{\sim}{\nabla}.(\rho \underset{\sim}{U}) = 0$$

$$(\underset{\sim}{U}.\nabla)\underset{\sim}{U} + \frac{1}{\rho} \underset{\sim}{\nabla}(\pi) = 0 \qquad (2.2)$$

$$\pi = \kappa \rho^{\gamma}, \quad c^2 = \frac{\gamma \pi}{\rho}$$

where

γ and κ are constants and $\gamma = c_p - c_v$.

When assumption 4 is used the mean flow should satisfy the viscous compressible equations. However, these are difficult to solve so often a boundary layer correction to an inviscid flow is used as a further approximation/assumption.

If the irrotational assumption is used equations (2.1) reduce to

$$\frac{i\omega}{c^2} + \underset{\sim}{\nabla}.(\rho\ \underset{\sim}{\nabla}\phi + \frac{1}{c^2}\ p\ \underset{\sim}{U}) = 0$$

$$\frac{i}{\rho}\ p + i\omega\phi + \underset{\sim}{U}.\underset{\sim}{\nabla}\phi = 0 \qquad (2.3)$$

where

ϕ is the acoustic velocity potential.

If assumption 1 is used the mean flow will satisfy,

$$\nabla(\rho\nabla\bar{\phi}) = 0$$

$$\rho = [\hat{\rho}^{\gamma-1} - \frac{\gamma-1}{2}\nabla\Phi.\nabla\Phi]^{\frac{1}{\gamma-1}} \qquad (2.4)$$

where

Φ is the mean flow velocity potential

$\hat{\rho}$ is the (constant) stagnation density.

When assumption 4 is used $(\hat{\rho},c,\underset{\sim}{U})$ represents the rotational mean flow.

BOUNDARY CONDITIONS

Since we are interested in the duct problem we consider the domains, Ω, to be of a specific form. We assume (see figure 1),

$$\partial\Omega = \Gamma_1 \cup \Gamma_2 \cup \Gamma_3 \cup \Gamma_4 \qquad (2.5)$$

where

$\Gamma_1 = \{(0,y): 0 < y < d_1\}$

= left hand end of the duct

$\Gamma_2 = \{(\ell,y): 0 < y < d_2\}$

= right hand end of the duct

Γ_3 = lower duct wall

Γ_4 = upper duct wall

d_1, d_2 are the duct widths at each end and ℓ is the duct length.

We assume that the duct walls are "hard". This requires that

$$\underset{\sim}{u}.n = 0 \quad \text{and} \quad \underset{\sim}{U}.n = 0$$

or (2.6)

$$\frac{\partial \phi}{\partial n} = 0 \quad \text{and} \quad \frac{\partial \Phi}{\partial n} = 0$$

on $\Gamma_3 \cup \Gamma_4$

where n is the unit outward normal to the duct.

It is interesting to note that when assumption 4 is used the mean flow will satisfy $\underset{\sim}{U} = \underset{\sim}{0}$ on the walls while the tangential acoustic velocity may or may not vanish.

It will be assumed that the duct terminates with semi-infinite uniform ducts which carry a uniform plug flow. In this situation, the solution in the duct, Ω, may be matched on to an analytical solution in the semi-infinite ducts. This solution, for the irrotational problem, is given by

$$\phi = \sum_{n=0}^{\infty} [a_n^+ \exp(\lambda_n^+ x) + a_n^- \exp(\lambda_n^- x)] \cos(\frac{n\pi}{d} y) \qquad (2.7)$$

$$\partial\Omega = \Gamma_1 \cup \Gamma_2 \cup \Gamma_3 \cup \Gamma_4$$

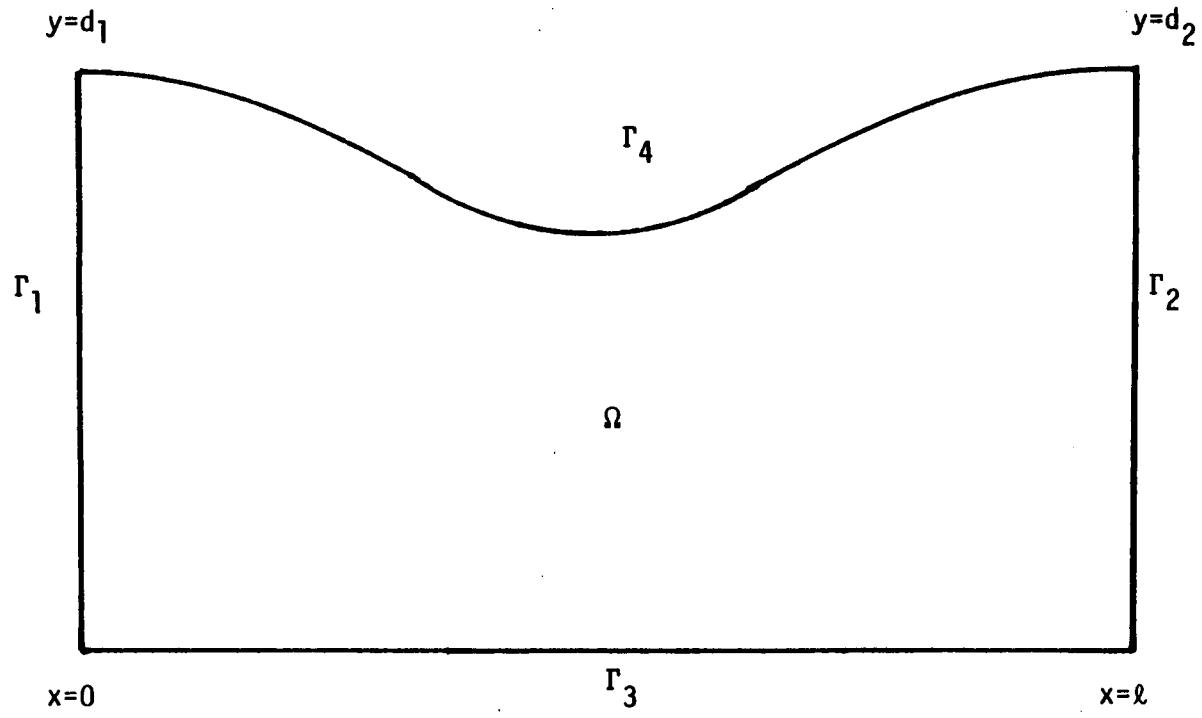

Figure 1. The duct computational domain.

where

d is the duct width

$\{a_n^+\}$, $\{a_u^-\}$ are arbitrary constants

$$\lambda_n^{\pm} = \frac{1}{1-M^2}\,(ikM \mp \delta_n)$$

$M = |\underset{\sim}{U}|/c$ = Mach. number of the mean flow

$k = \frac{\omega}{c}$ = spatial wave number

$$\delta_n = i[k^2 - (1-M^2)(\tfrac{n\pi}{d})^2]^{\frac{1}{2}}$$

When rotational disturbances are permitted the uniform duct solution is

$$\begin{bmatrix} p \\ u \\ v \end{bmatrix} = \sum_{n=0}^{\infty} \begin{bmatrix} \cos(\frac{n\pi}{d}\,y) & & \\ & \cos(\frac{n\pi}{d}\,y) & \\ & & \sin(\frac{n\pi}{d}\,y) \end{bmatrix} [A_n] \begin{bmatrix} a_n^+ \exp(\lambda_u^+ x) \\ a_n^- \exp(\lambda_n^- x) \\ a_n^0 \exp(\lambda_n^0 x) \end{bmatrix} \qquad (2.8)$$

where

$$[A_n] = \left[\begin{array}{c|c|c} 1 & 1 & 0 \\ \hline \dfrac{-\lambda_n^+}{\rho c(ik + \lambda_n^+ M)} & \dfrac{-\lambda_n^-}{\rho c(ik + \lambda_n^- M)} & \dfrac{M}{k}(\tfrac{n\pi}{k}) \\ \hline (\tfrac{n\pi}{d})\dfrac{1}{\rho c(ik + \pi_n^+ M)} & (\tfrac{n\pi}{d})\dfrac{1}{\rho c(ik + \lambda_n^- M)} & i \end{array}\right]$$

$\{a_n^+\}$, $\{a_n^-\}$ and $\{a_n^0\}$ are amplitude coefficients

$\lambda_n^{\pm}$ are as in equation (2.7)

$$\lambda_n^0 = -\frac{ik}{M}$$

The last column of the coefficient matrix $[A_n]$ introduces the rotational part of the disturbance. Similar representations are used at $x = \ell$, with $[A_n]$ replaced by $[B_n]$ and the a_n replaced by b_n.

The quantities $\{a_n^+\}$ and $\{a_n^-\}$ represent wave amplitudes of waves moving in the positive and negative directions respectively. The $\{a_n^0\}$ are the amplitudes of hydrodynamic waves that move with the mean flow and do not exist if the flow is irrotational. At the duct terminations we require the solution within the duct to match the above analytical solution. In particular we require

$$(\rho\nabla\phi + \frac{1}{c^2}\underset{\sim}{U}\, p)\cdot \hat{\underset{\sim}{n}}\,\Big|_{(0,y)} = \rho_1 \sum_{n=0}^{\infty} \delta_n^1 (a_n^+ - a_n^-)\, \mathrm{Cos}(\frac{n\pi}{d_1} y) \tag{2.9}$$

$$(\rho\nabla\phi + \frac{1}{c^2}\underset{\sim}{U}\, p)\cdot \hat{\underset{\sim}{n}}\,\Big|_{(\ell,y)} = -\rho_2 \sum_{n=0}^{\infty} \delta_n^2 (b_n^+ - b_n^-)\, \mathrm{Cos}(\frac{n\pi}{d_2} y)$$

or, when potential flow is not enforced

$$(\rho\underset{\sim}{u} + \frac{1}{c^2} p\, \underset{\sim}{U})\cdot \hat{\underset{\sim}{n}}\,\Big|_{(0,y)} = \sum_{n=0}^{\infty} [\frac{\delta_n}{c(ik + \lambda_n^+ M)} a_n^+ - \frac{\delta_n}{c(ik + \lambda_n^- M)} a_n^-$$

$$+ \frac{\rho M}{k} (\frac{n\pi}{d_1})\, a_n^0]_{\Gamma_1}\, \mathrm{Cos}(\frac{n\pi}{d_1} y) \tag{2.10}$$

$$(\rho\underset{\sim}{u} + \frac{1}{c^2} p\, \underset{\sim}{U})\cdot \hat{\underset{\sim}{n}}\,\Big|_{(\ell,y)}$$

$$= \sum_{n=0}^{\infty} [\frac{\delta_n}{c(ik + \lambda_n^+ M)} b_n^+ - \frac{\delta_n}{c(ik + \lambda_n^- M)} b_n^- + \frac{\rho M}{k} (\frac{n\pi}{d_2}) b_n^0]_{\Gamma_2}\, \mathrm{Cos}(\frac{n\pi}{d_2} y)$$

Where in equations (2.10) the subscripts Γ_1 and Γ_2 indicate that the quantities appearing within the brackets are to be evaluated on Γ_1 and Γ_2 respectively.

We specify the waves incident upon the duct, Ω. This corresponds to specifying $\{a_n^+\}$, $\{b_n^-\}$ and $\{b_n^0\}$ if the mean flow Mach number is negative (specify $\{a_n^0\}$ if $M > 0$).

If the duct terminations are not in regions of uniform plug flow, no analytical solutions corresponding to equations (2.7) and (2.8) exist.

Astley and Eversman [14] proposed a method for generalising these modal boundary conditions. However some technical problems arise with this approach so only plug flows are considered here.

III. WEAK PROBLEMS

In this section we discuss several weak formulations used for the modelling of the duct problem. We first discuss a formulation using an acoustic velocity potential. The other two weak formulations, based upon the primative form of the equations, are those pursued by Astley and Eversman [2-3] and Abrahamson [6-7] respectively.

1. Velocity Potential Formulation

In order to incorporate the modal boundary conditions of equation (2.9) into the problem it is necessary to define a space of sequences, S, which are square summable in a weighted sense. Let

$$S = \{a: \; a_0^2 + \sum_{n=1}^{\infty} |a_n|^2 n < \infty\} \tag{3.1}$$

The modal amplitudes at the left and right hand ends of the duct will be denoted by (a^+,a^-) and (b^+,b^-) respectively and will be required to lie in S x S (i.e. $a^+ \varepsilon S$ and $a^- \varepsilon S$, etc.). The sequences of eigenvalues of the ends of the duct are denoted by (λ^+,λ^-). In formulating the weak problem we will need certain spaces. First recall that $L^2(\Omega)$ defines the linear space of equivalence classes of measurable functions g such that $\int_\Omega |g|^2 < \infty$ and that $H^1(\Omega)$ defines the linear space of equivalence classes of functions in $L^2(\Omega)$ whose first distributed derivatives are also in $L^2(\Omega)$. The weak problem may now be stated. Find $(\phi,p,a^-,b^+) \varepsilon H^1(\Omega) \times L^2(\Omega) \times S \times S$ such that

$$\text{(i)} \quad \int_\Omega \{-\frac{i\omega}{c^2} p\,\bar{\psi} = (\rho \underset{\sim}{\nabla}\phi + \frac{1}{c^2} p\,\underset{\sim}{U}).\underset{\sim}{\nabla}\bar{\psi}\}$$

$$- \rho_1 \sum_{n=0}^{\infty} (a_n^+ - a_n^-)\,\delta_n^1 \int_{\Gamma_1} \text{Cos}(\frac{n\pi}{d_1} y)\,\bar{\psi} \tag{3.2a}$$

$$+ \rho_2 \sum_{n=0}^{\infty} (b_n^+ - b_n^-)\,\delta_n^2 \int_{\Gamma_2} \text{Cos}(\frac{n\pi}{d_2} y)\,\bar{\psi} = 0$$

$$\text{(ii)} \quad \int_\Omega \{\frac{1}{\rho} p.\; \underset{\sim}{U}.\underset{\sim}{\nabla}\phi + i\omega\phi\}\bar{q} = 0 \tag{3.2b}$$

$$\text{(iii)}\quad \sum_{n=1}^{\infty} n\{\frac{2}{d_1}(a_n^+ + a_n^-) - \int_{\Gamma_1} \phi \cos(\frac{n\pi}{d_1} y)\}\bar{\alpha}_n + \{\frac{1}{d_1}(a_0^+ + a_0^-) - \int_{\Gamma_1} \phi\}\bar{\alpha}_0 = 0 \tag{3.2c}$$

$$\text{(iv)}\quad \sum_{n=1}^{\infty} n\{\frac{2}{d_2}(b_n^+ + b_n^-) - \int_{\Gamma_2} \phi \cos(\frac{n\pi}{d_2} y)\}\bar{p}_n + \{\frac{1}{d_2}(a_0^+ + a_0^-) - \int_{\Gamma_2} \phi\}\beta_0 = 0 \quad \forall (\psi,q,\alpha,\beta) \in H^1(\Omega) \times L^2(\Omega) \times S \times S \tag{3.2d}$$

In the statement of this weak problem $(\rho,c,\underset{\sim}{U})$ is the mean flow, a^+ and b^- are presumed to be given and ρ_1, d_1 and ρ_2, d_2 are the values of the mean flow density and duct widths at the left and right hand ends of the duct respectively. The quantities δ_n^1 and δ_n^2 are the radicals defined in equation (2.7), evaluated at the left and right hand ends of the duct respectively.

It is shown in Appendix I that this weak problem is well posed under a physically reasonable hypothesis on the mean flow.

We have chosen to solve for the pressure explicitly. As an alternative the velocity potential could be calculated initially by eliminating the pressure and then the pressures calculated subsequently.

2. Astley Eversman Formulation

The modeling of the modal boundary conditions (equations (2.9-2.10) is more involved when the primative equations are utilized. Astley and Eversman proposed the following ideas to accomplish this.

For each $(p,\underset{\sim}{u}) \in H^1(\Omega) \times H^1(\Omega)^2$ define six sequences a^+, a^-, a^0, b^+, b^-, b^0 where

$$\begin{bmatrix} a_n^+ \\ a_n^- \\ a_n^0 \end{bmatrix} = [A_n]^{-1} \frac{2}{d_1} \int_{\Gamma_1} \begin{bmatrix} \cos(\frac{n\pi}{d_1} y) & & \\ & \cos(\frac{n\pi}{d_1} y) & \\ & & \cos(\frac{n\pi}{d_1} y) \end{bmatrix} \begin{bmatrix} p \\ u_1 \\ u_2 \end{bmatrix} \tag{3.3a}$$

$$\begin{bmatrix} b_n^+ \\ b_n^- \\ b_n^0 \end{bmatrix} = [B_n]^{-1} \frac{2}{d_2} \int_{\Gamma_2} \begin{bmatrix} \cos(\frac{n\pi}{d_2} y) & & \\ & \cos(\frac{n\pi}{d_2} y) & \\ & & \cos(\frac{n\pi}{d_2} y) \end{bmatrix} \begin{bmatrix} p \\ u_1 \\ u_2 \end{bmatrix} \tag{3.3b}$$

for n=1,2,3 with $a_0^0 = b_0^0 = 0$

$$\begin{bmatrix} a_0^+ \\ a_0^- \end{bmatrix} = \begin{bmatrix} 1 & 1 \\ -\lambda_0^+ & -\lambda_0^- \\ \hline \rho c(ik + \lambda_0^+ M) & \rho c(ik + \lambda_0^- M) \end{bmatrix}_{\Gamma_1}^{-1} \frac{1}{d_1} \int_{\Gamma_1} \begin{bmatrix} p \\ u_1 \end{bmatrix} \tag{3.4a}$$

$$\begin{bmatrix} b_0^+ \\ b_0^- \end{bmatrix} = \begin{bmatrix} 1 & 1 \\ -\lambda_0^+ & -\lambda_0^- \\ \hline \rho c(ik + \lambda_0^+ M) & \rho c(ik + \lambda_0^- M) \end{bmatrix}_{\Gamma_2}^{-i} \frac{1}{d_2} \int_{\Gamma_2} \begin{bmatrix} p \\ u_1 \end{bmatrix} \tag{3.4b}$$

We now fix some notation so that the space of solutions may be defined. For $w = (p,\underset{\sim}{u}) \in H^1(\Omega) \times H^1(\Omega)^2$ define

$$A^+ : H^1(\Omega) \times H^1(\Omega)^2 \to \ell^2$$

by

$$A^+(w) = a^+$$

where a^+ is defined in equation (3.3). Similarly we difine A^-, A^0, B^+, B^-, and B^0.

Let a^+, b^-, b^0 be specified. The function spaces of Astley and Eversman are:

$$\mathcal{U} = \{w \in H^1(\Omega) \times H^1(\Omega)^2 : A^+(w) = a^+, B^-(w) = b^-, \quad B^0(w) = b^0\} \tag{3.6}$$

$$\mathcal{U}_0 = \{w \in H^1(\Omega) \times H^1(\Omega)^2 : A^+(w) = B^-(w) = B^0(w) = 0\} \tag{3.7}$$

with the weak problem becoming:

Find $(p, \underset{\sim}{u}) \in \mathcal{U}$ such that

$$\text{(i)} \quad \int_\Omega \{\frac{-i\omega}{c^2} p\bar{q} + (\rho \underset{\sim}{u} + \frac{1}{c^2} \underset{\sim}{U} p) \cdot \underset{\sim}{\nabla}\bar{q}\}$$

$$- \sum_{n=0}^{\infty} \{\frac{\delta_n^1}{c(ik + \lambda_n^+ M)} a_n^+ - \frac{\delta_n^1}{c(ik + \lambda_n^- M)} a_n^- + \frac{P_1 M}{k} (\frac{n\pi}{d_1}) a_n^0\}_{\Gamma_1} \tag{3.8a}$$

$$\cdot \int_{\Gamma_1} \cos(\frac{n\pi}{d_1} y)\, \bar{q}$$

$$+ \sum_{n=0}^{\infty} \{\frac{\delta_n^2}{c(ik + {}^+_n M)} b_n^+ - \frac{\delta_n^2}{c(ik + {}^-_n M)} b_n^- + \frac{\rho_2 M}{K} (\frac{n\pi}{d_2}) b_n^0\}_{\Gamma_2}$$

$$\cdot \int_{\Gamma_2} \cos(\frac{n\pi}{d_2} y)\, \bar{q} = 0$$

$$\text{(ii)} \quad \int_\Omega \{i\omega \underset{\sim}{u} + (\underset{\sim}{U} \cdot \underset{\sim}{\nabla}) \underset{\sim}{u} + (\underset{\sim}{u} \cdot \underset{\sim}{\nabla}) \underset{\sim}{U} + \underset{\sim}{\nabla}(\frac{p}{\rho})\} \cdot \underset{\sim}{\bar{v}} = 0 \tag{3.8b}$$

$$\forall\ (q, \underset{\sim}{v}) \in \mathcal{U}$$

Here it is understood that a^+, b^- and b^0 are data with $a^- = A^-(p,u)$, $b^- = B^+(p,u)$, and $a^0 = A^0(p,u)$.

3. Abrahamson Weak Problem

Abrahamson [6] used the following weak problem for his ADAM computer program. Let

$$\mathcal{V} = \{(p,\underset{\sim}{u}) \in U: \ \underset{\sim}{u}.\underset{\sim}{n}|_{\Gamma_3} = \underset{\sim}{u}.\underset{\sim}{n}|_{\Gamma_4} = 0\} \tag{3.9}$$

$$\mathcal{V}_0 = \mathcal{V} \cap U_0,$$

then find $(p,u) \in \mathcal{V}$ such that

$$\int_\Omega \{\frac{i\omega}{c^2} p + \underset{\sim}{\nabla}.(\rho \underset{\sim}{u} + \frac{1}{c^2} \underset{\sim}{U} p)\}\bar{q} = 0 \tag{3.10a}$$

$$\int_\Omega \{i\omega\underset{\sim}{u} + (\underset{\sim}{U}.\underset{\sim}{\nabla})\underset{\sim}{u} + (\underset{\sim}{u}.\underset{\sim}{\nabla})\underset{\sim}{U} + \underset{\sim}{\nabla}(\frac{p}{\rho})\}.\bar{\underset{\sim}{v}} = 0 \quad \forall (q,\underset{\sim}{v}) \in \mathcal{V}_0. \tag{3.10b}$$

IV. FINITE ELEMENT APPROXIMATION OF THE WEAK PROBLEMS

1. Velocity Potential Formulation

The function spaces $H^1(\Omega)$ and $L^2(\Omega)$ from which ϕ and p are chosen may be approximated by the usual finite element subspaces, $\mathbb{M}_k^0(\Omega)$ and $\mathbb{M}_\ell^{-1}(\Omega)$. The superscript is used to indicate the degree of inter-element continuity (0 continuous, -1 discontinuous) and the subscript indicates the degree of polynomial used in the construction of each element. To approximate the sequences the following finite dimensional subspaces are utilized.

$$S_N = \{a \in S: a_n = 0 \quad \forall\ n > N\} \tag{4.1}$$

The approximate weak problem is then; Find $(\phi,p,a^-,b^+) \in \mathbb{M}_k^0(\Omega) \times \mathbb{M}_\ell^{-1}(\Omega) \times S_N \times S_N$ such that equations (3.2a-d) hold $\forall\ (\psi,q,\alpha,\beta) \in \mathbb{M}_k^0(\Omega) \times \mathbb{M}^{-1}(\Omega) \times S_N \times S_N$.

Under certain technical assumptions it is shown in Appendix 1, that if,

(i) $\ell \geq k-1$

(ii) $N \geq \frac{1}{h}$ where h is the maximum diameter of the elements used in the finite element triangulation,

then,

$$\begin{aligned} |\phi - \phi_0|_1 &\leq c_1 h^k \\ |p - p_0|_0 &\leq c_2 h^k \quad (c_1,\ c_2 \text{ constants}) \end{aligned} \tag{4.2}$$

where (ϕ_0,p_0) is the solution and (ϕ,p) is the approximate solution. In other words the finite element scheme converges with an optimal rate if suitable care is given to a required compatibility between the approximation for the velocity potential and the pressure and boundary coefficients.

2. Astley-Eversman Algorithm

It is not immediately obvious how the class of functions U discussed in section III.2 may be approximated. Astley and Eversman [3] proposed the following algorithm to generate (non-conforming) approximations.

Let $M_k^0(\Omega) \times M_k^0(\Omega)^2 \in H^1(\Omega) \times H^1(\Omega)^2$ be the usual finite element subspaces as described in section IV.1 above. On Γ_1 the trace of any element $(\underset{\sim}{u},p) \in M_k^0(\Omega) \times M_k^0(\Omega)^2$ may be written as

$$\begin{bmatrix} p \\ u_1 \\ u_2 \end{bmatrix}\Bigg|_{\Gamma_1} = \sum_{i=1}^{M} \begin{bmatrix} \Phi_i & & \\ & \Phi_i & \\ & & \Phi_i \end{bmatrix} \begin{bmatrix} p \\ u_1 \\ u_2 \end{bmatrix}_i \tag{4.3}$$

where $\begin{bmatrix} p \\ u_1 \\ u_2 \end{bmatrix}_i$ correspond to the function values of $\begin{bmatrix} p \\ u_1 \\ u_2 \end{bmatrix}$ at node i on Γ_1 and Φ_i are the interpolation functions corresponding to node i on Γ_1. The nodal values of (p,u) are then constrained to satisfy,

$$\int_{\Gamma_1} \begin{bmatrix} \Phi_j & & \\ & \Phi_j & \\ & & \Phi_j \end{bmatrix} \sum_{i=1}^{M} \begin{bmatrix} \Phi_i & & \\ & \Phi_i & \\ & & \Phi_i \end{bmatrix} \begin{bmatrix} p \\ u_1 \\ u_2 \end{bmatrix}_i$$

$$= \sum_{n=0}^{N} \int_{\Gamma_1} \begin{bmatrix} \Phi_j & & \\ & \Phi_j & \\ & & \Phi_j \end{bmatrix} [A_n] \begin{bmatrix} \cos(\frac{n\pi}{d_1} y) & & \\ & \cos(\frac{n\pi}{d_1} y) & \\ & & \cos(\frac{n\pi}{d_1} y) \end{bmatrix} \begin{bmatrix} a_n^+ \\ a_n^- \\ a_n^0 \end{bmatrix} \tag{4.4}$$

for all j = 1,2, ... M. N represents the number of modal amplitudes being used in the approximation, and $[A_n]$ is the matrix defined in equation (2.8). Equation (4.4) gives a relationship between the modal amplitudes and the nodal values on the boundary for the approximation. This relation may be written

$$\underset{\sim}{U}_0 = [T_0]\ \underset{\sim}{A} \tag{4.5a}$$

where $\underset{\sim}{U}_0$ corresponds to the nodal values of $(p,\underset{\sim}{u})$ on Γ_1 and $\underset{\sim}{A}$ the vector of nodal amplitudes $(a_n^+, a_n^-, a_n^0, n = 1,2,\ldots N)$. An analogous expression for the nodal values on Γ_2 may be written as

$$\underset{\sim}{U}_\ell = [T_\ell]\ \underset{\sim}{B}. \tag{4.5b}$$

If a typical element of $M_k^0(\Omega) \times M_k^0(\Omega)^2$ is described by

$$\begin{bmatrix} p \\ u_1 \\ u_2 \end{bmatrix} = [\Phi] \begin{bmatrix} \underset{\sim}{U}_0 \\ \underset{\sim}{U} \\ \underset{\sim}{U}_\ell \end{bmatrix} \tag{4.6}$$

where $\underset{\sim}{U}_0$ and $\underset{\sim}{U}_\ell$ are the nodal values on Γ_1 and Γ_2 and $\underset{\sim}{U}$ contains the other nodal values a typical element of the space used to approximate U would described by

$$\begin{bmatrix} p \\ u_1 \\ u_2 \end{bmatrix} = [\Phi] \begin{bmatrix} \underset{\sim}{T}_0 & & \\ & \underset{\sim}{I} & \\ & & \underset{\sim}{T}_\ell \end{bmatrix} \begin{bmatrix} \underset{\sim}{A} \\ \underset{\sim}{U} \\ \underset{\sim}{B} \end{bmatrix} \tag{4.7}$$

where I is an identity matrix and $[T_0]$, $[T_\ell]$ are as in equation (4.5). The constraints on a^+, b^-, etc. can now easily be implemented using penalisation. Astley and Eversman [7] describe the implementation of this algorithm in detail.

V. RESULTS

1. Uniform Duct Results

The analytical solution to the acoustic problem for a uniform duct carrying a uniform mean flow was given in equations (2.7-2.8). This provides a test case which can be used to estimate how well the finite element approximations do approximate the solution. Throughout this section we use the L^2 norm of the error in pressure, defined by,

$$|p - p_h|_0^2 = \int_\Omega |p - p_h|^2$$

where

p = analytical solution

p_h = finite element solution,

to estimate the error in the solution. Standard results [15] show that a finite element approximation using polynomials of degree k would have an optimal rate of convergence in the L^2 norm of order k+1, i.e.

$$|p - p_h|_0 \leq c\, h^{k+1}$$

where

h = diameter of largest element,

if the solution sought was sufficiently smooth. Fix, Nicolaides, and Gunzburger [11] obtained optimal convergence for the no flow case using their least squares scheme with linear triangles (k=1) on a "criss cross" grid (i.e. a grid satisfying the grid decomposition property [10]).

Potential Flow Code:

We consider the potential flow code separately from the other two algorithms for two reasons. First, we have the analytical results in the Appendix that indicate that the finite element scheme should converge optimally when quadratic elements are used for the velocity potential and discontinuous linear elements are used for the pressure. Secondly, the results indicate that extremely 'rough' mean flows are admissible since no mean flow derivatives enter this problem.

When the finite element approximation described in equations (3.2) was used to solve for the analytical solution given in equation (2.7) optimal convergence of the pressure was observed in all cases tried. This was expected since the analytical solution has infinitely many derivatives. A more interesting example may be constructed by combining two of the solutions given in equation (2.7) with different mean flows. (See Figure 2) This results in a problem with a discontinuity in the mean flow and the acoustic pressure, the velocity potential being continuous. The compatibility condition at the interface may be written as

$$[\![(\rho u + \frac{1}{c^2} \underset{\sim}{\nabla} p) \cdot \underset{\sim}{e}_x]\!] (0.5) = 0$$

We consider the results using the following as data:

$$\omega = 1.0, \quad a_0^+ = 1.0 \quad a_n^+ = 0, \quad n=1,2,\ldots, \quad \ell=1.0, \quad d = 0.5$$

$$c = 1.0, \quad b_0^- = 0 \qquad n = 0,1,2,\ldots.$$

$$\rho(x,y) = \begin{array}{ll} 1.0 & \text{if } x < 0.5 \\ 0.5 & \text{if } x \geq 0.5 \end{array} \qquad \underset{\sim}{U} = \begin{array}{ll} -0.25\, \underset{\sim}{e}_x & x < 0.5 \\ -0.5\, \underset{\sim}{e}_x & x \geq 0.5 \end{array}$$

The choice of a plane wave incident at x=0 ($a_0^+ = 1$) is presented so that the jump in pressure at the interface can easily be plotted. Calculations were made with non plane waves and the results were essentially the same.

Figure 3 shows the real part of the pressure plotted near x=0.5 that was calculated using a mesh with 10 uniformly spaced elements across the duct and 20 elements along the duct (a 10 x 20 mesh). This solution almost exactly overlays the analytical solution. It can be seen that the jump is captured without any of the characteristic wiggles associated with ill-posed problems. It is interesting to note that while the pressures away from the discontinuity could be discontinuous, the solution has almost no jumps at the other element interfaces. The 10 x 20 mesh used for figure 3 has element boundaries along the interface x=0.5, so the jump can be captured exactly. If a 10 x 21 element mesh is used the discontinuity can no longer be captured exactly since the jump in pressure does not coincide with element boundaries. The solution for the real part of the pressure near x=0.5 obtained with a 10 x 21 mesh is given in figure 4. It can be seen that in this situation the pressure in the element centered at x=0.5 simply stradles the jump and otherwise the pressure is still very accurate. It is possible to use elements with continuous pressures to solve this problem. This was done for both the 10 x 20 and 10 x 21 element meshes and the pressures are plotted in figure 5 and 6. The error associated with the discontinuity appears to spread over at least three elements for each of these solutions.

A plot of the L^2 error in the pressure versus mesh size (h) is given in figure 7. When discontinuous elements were used that had boundaries on x=0.5 the convergence rate is optimal (slope = 2). The other two lines

with slope = 1 are the convergence curves for the case where the interface x=0.5 always bisectes an element so that the jump couldn't be calculated exactly and the case where the pressures were continuous. Since this problem does not have a smooth solution the approximation results given in the Appendix do not apply and this explains why even the discontinous pressures may give sub-optimal convergence rates.

ASTLEY AND ABRAHAMSON CODES:

The weak problems presented in equations (3.8) and (3.10) both involve derivatives of the mean flow so discontinuous mean flows, like the one discussed for the potential flow code, can not be considered. In order to investigate the behavior of the two algorithms, a uniform duct case was considered; the solution being given in equation (2.8). Since the solutions were all continuous it is possible to calculate the H^1 error of the solution defined by:

$$| p - p_h |_1^2 = \int_\Omega \{ |p - p_h|^2 + |\underset{\sim}{\nabla}(p - p_h)|^2 \}$$

where

p = analytical solution

p_h = finite element solution

Standard results show that if the solution sought is smooth, and polynomials of degree k are used to construct the finite element mesh approximating the solution, the optimal H^1 rate of convergence is k, i.e.

$$| p - p_h |_1 \leq c\, h^k$$

Error calculations were made using both the L^2 and H^1 norms.

The following data are used for the uniform duct problems considered.

$\omega = 1.0, \quad \ell = 1.0, \quad d = 0.5$

$\underset{\sim}{U} = -0.5\, \underset{\sim}{e}_x \quad \rho = 1.0, \quad c = 1.0$

$a_0^+ = b_0^- = 0, \quad a_n^+ = b_n^0 = 0 \quad n = 2,3,\ldots \quad b_n^- = 0 \quad n = 0,1,\ldots$

Two cases are discussed, the first has a wave of unit amplitude incident at x=0 corresponding to the first transverse mode ($a_1^+ = 1.0$), and the second case considers a wave of unit amplitude incident at x=1.0 corresponding to the first hydrodynamic mode ($b_1^0 = 1.0$). This latter case has no correspondence in the irrotational model so the primitive form of the equations must be used to solve for this solution. For each of the two algorithms eight noded isoparametric elements were used for both the pressure and velocity. Optimal rates of convergence would then be 2 in the H^1 norm and 3 in the L^2 norm.

Figures 8 and 9 are plots of the H^1 and L^2 errors in velocity and pressure respectively, verses mesh size for the first problem. For this problem both algorithms gave (approximately) the same convergence rates, however these rates are not optimal. The rates were one and two for H^1 and L^2 errors respectively. This is precisely one less than optimal. Astley's algorithm consistently gave errors that were smaller than those given by Abrahamson's algorithm. The results for the second problem are shown in figures 10 and 11. These curves show that Astley's algorithm still gave at least the same rates as for the first problem while Abrahamson's algorithm converged slower (in the pressure) for this problem, demonstrating that Abrahamson's code has convergence rates that are problem dependent.

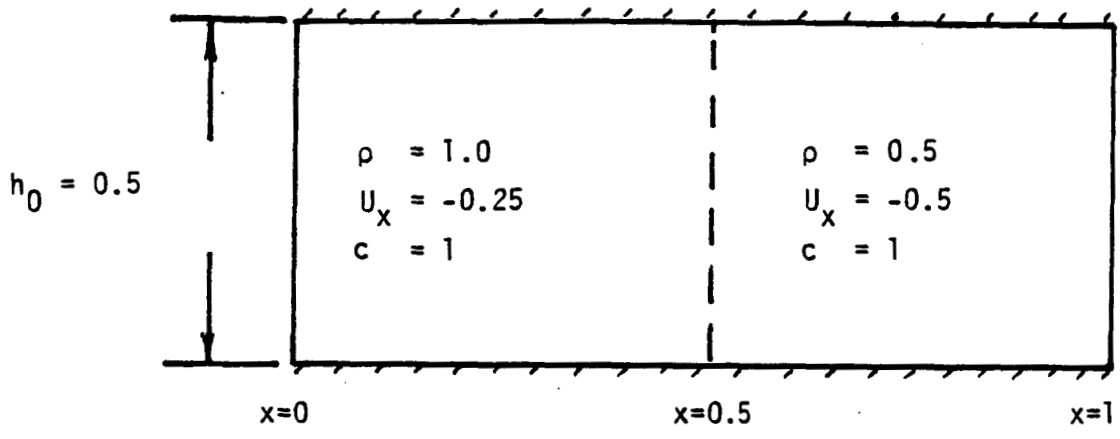

$$\omega = 1.0$$

$$a_0^+ = 1.0 \qquad a_n^+ = 0 \qquad n > 0$$

$$b_n^- = 0 \qquad \forall n = 0,1,\ldots$$

$$\phi_n\big|_{\Omega e} \in P_2 \quad \text{ie} \quad k = 2$$

$$P_n\big|_{\Omega e} \in P_1 \quad \text{ie} \quad \ell = 1$$

Figure 2. Schematic of the uniform duct test case with discontinuous flow (non-physical).

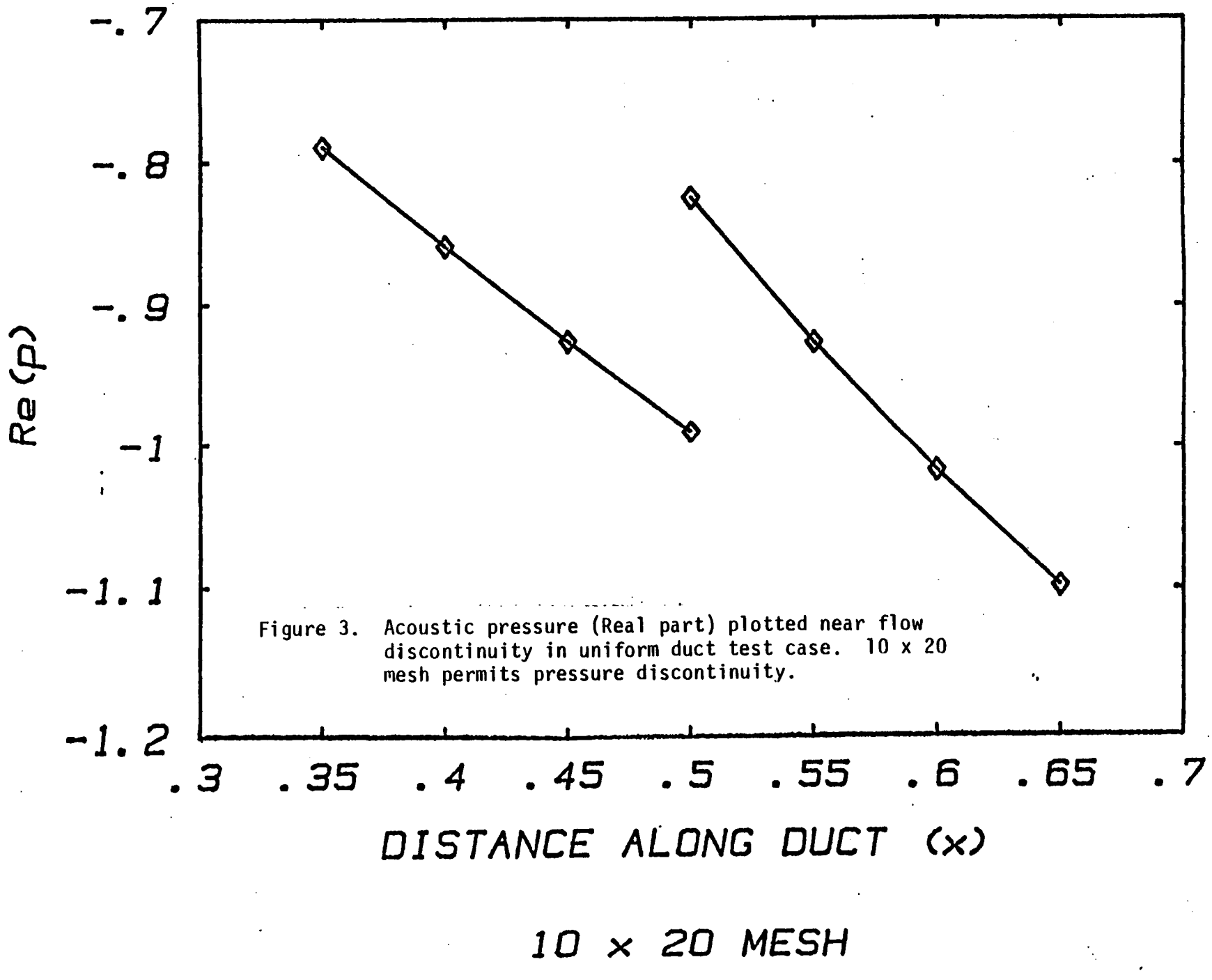

Figure 3. Acoustic pressure (Real part) plotted near flow discontinuity in uniform duct test case. 10 x 20 mesh permits pressure discontinuity.

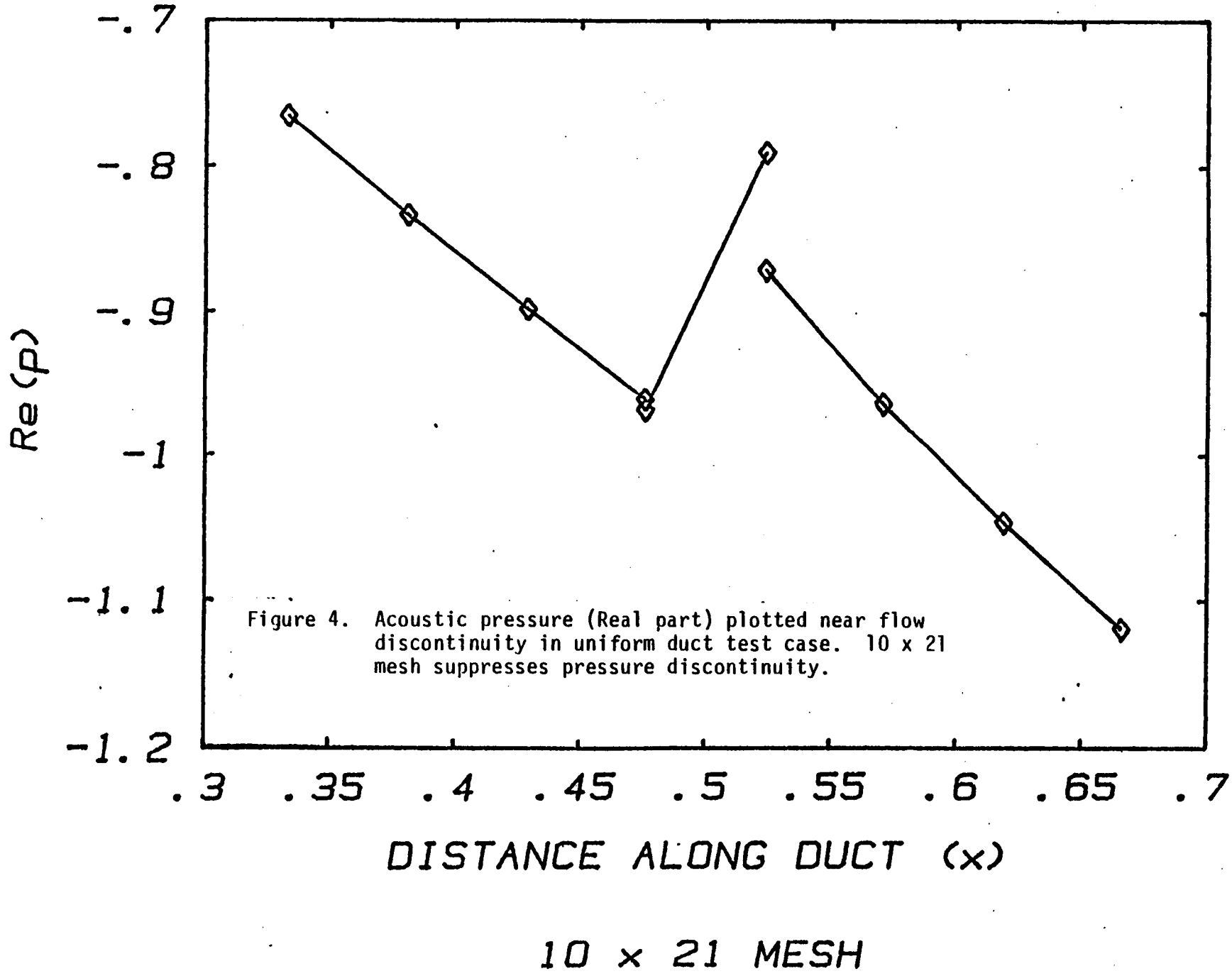

Figure 4. Acoustic pressure (Real part) plotted near flow discontinuity in uniform duct test case. 10 x 21 mesh suppresses pressure discontinuity.

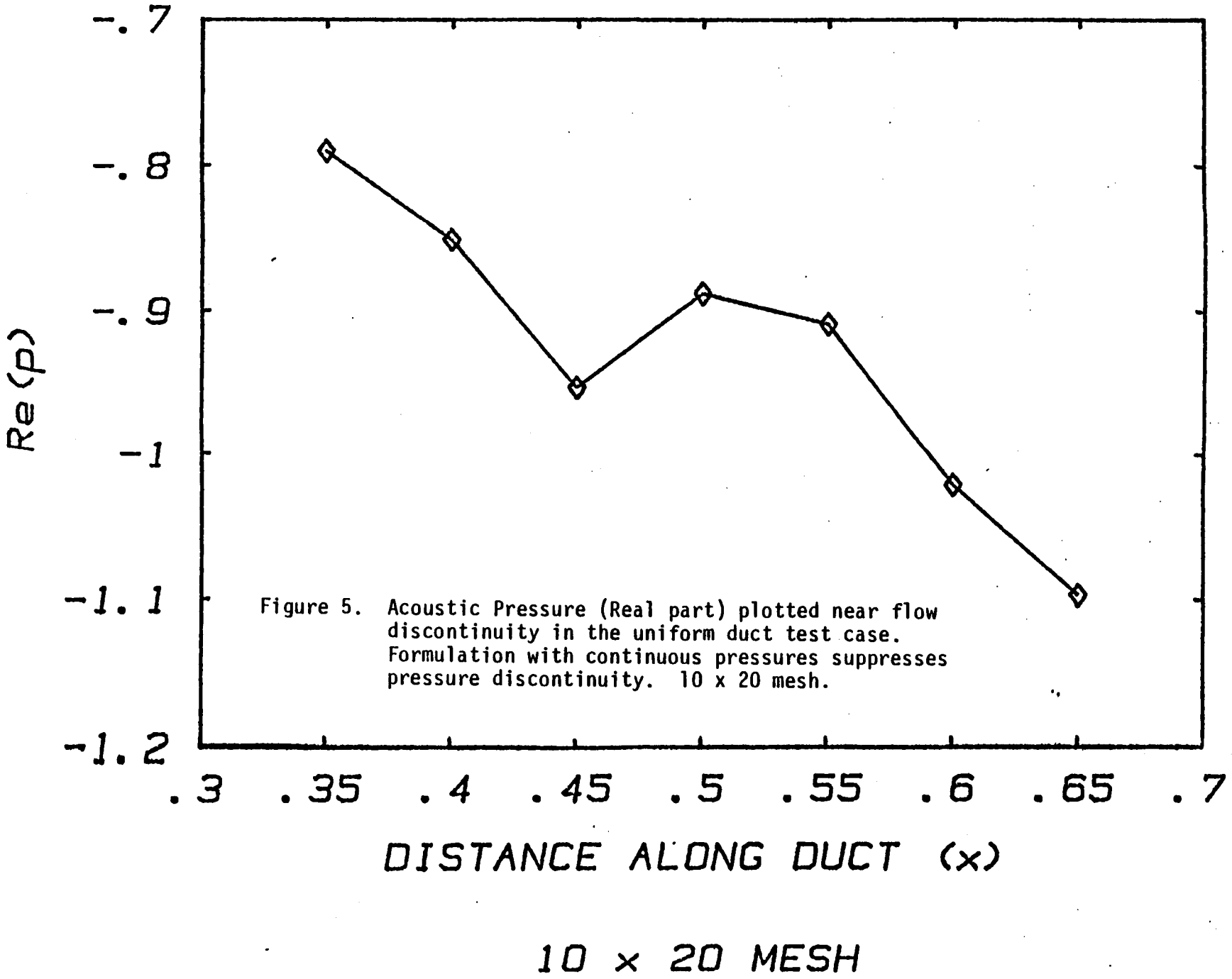

Figure 5. Acoustic Pressure (Real part) plotted near flow discontinuity in the uniform duct test case. Formulation with continuous pressures suppresses pressure discontinuity. 10 x 20 mesh.

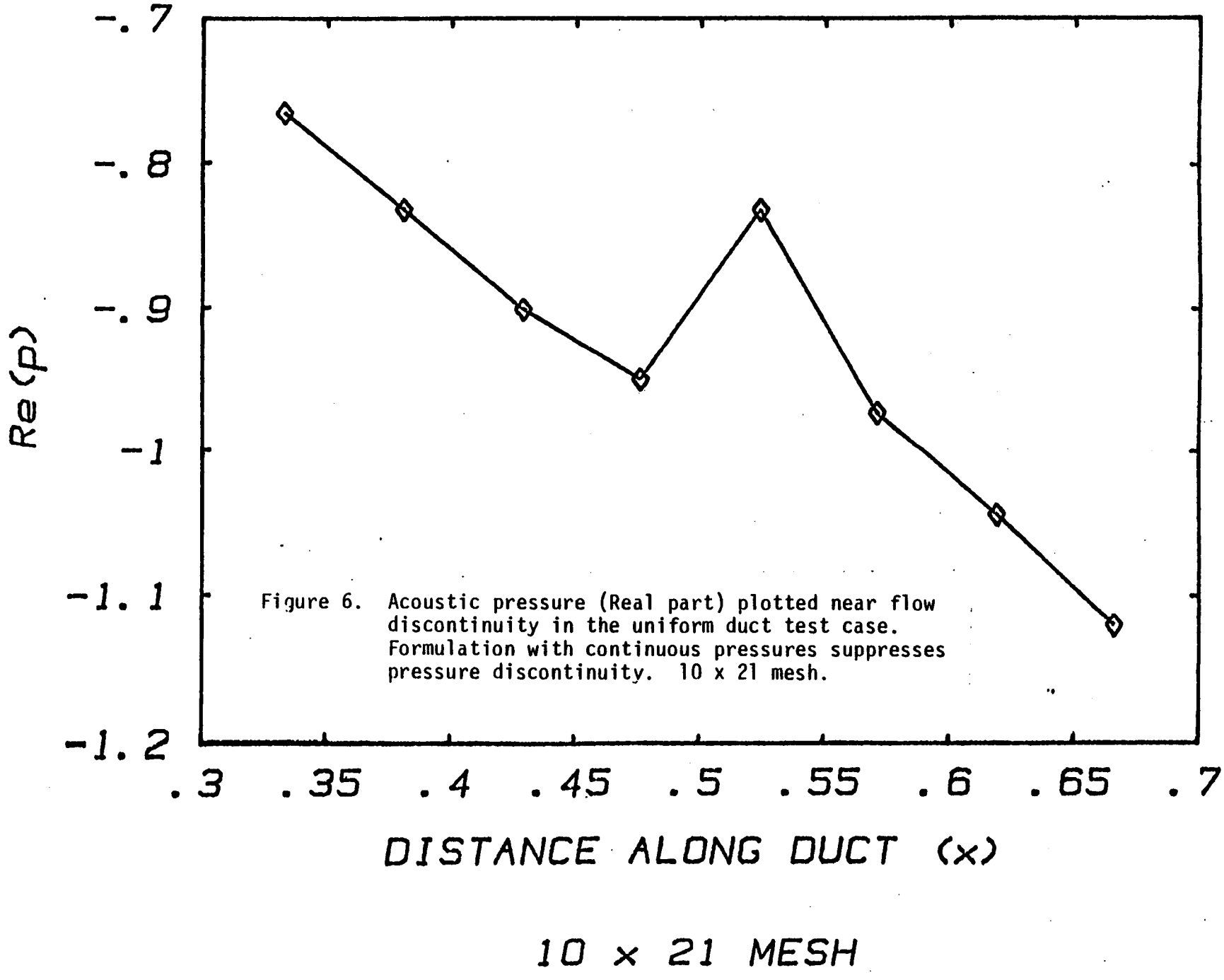

Figure 6. Acoustic pressure (Real part) plotted near flow discontinuity in the uniform duct test case. Formulation with continuous pressures suppresses pressure discontinuity. 10 x 21 mesh.

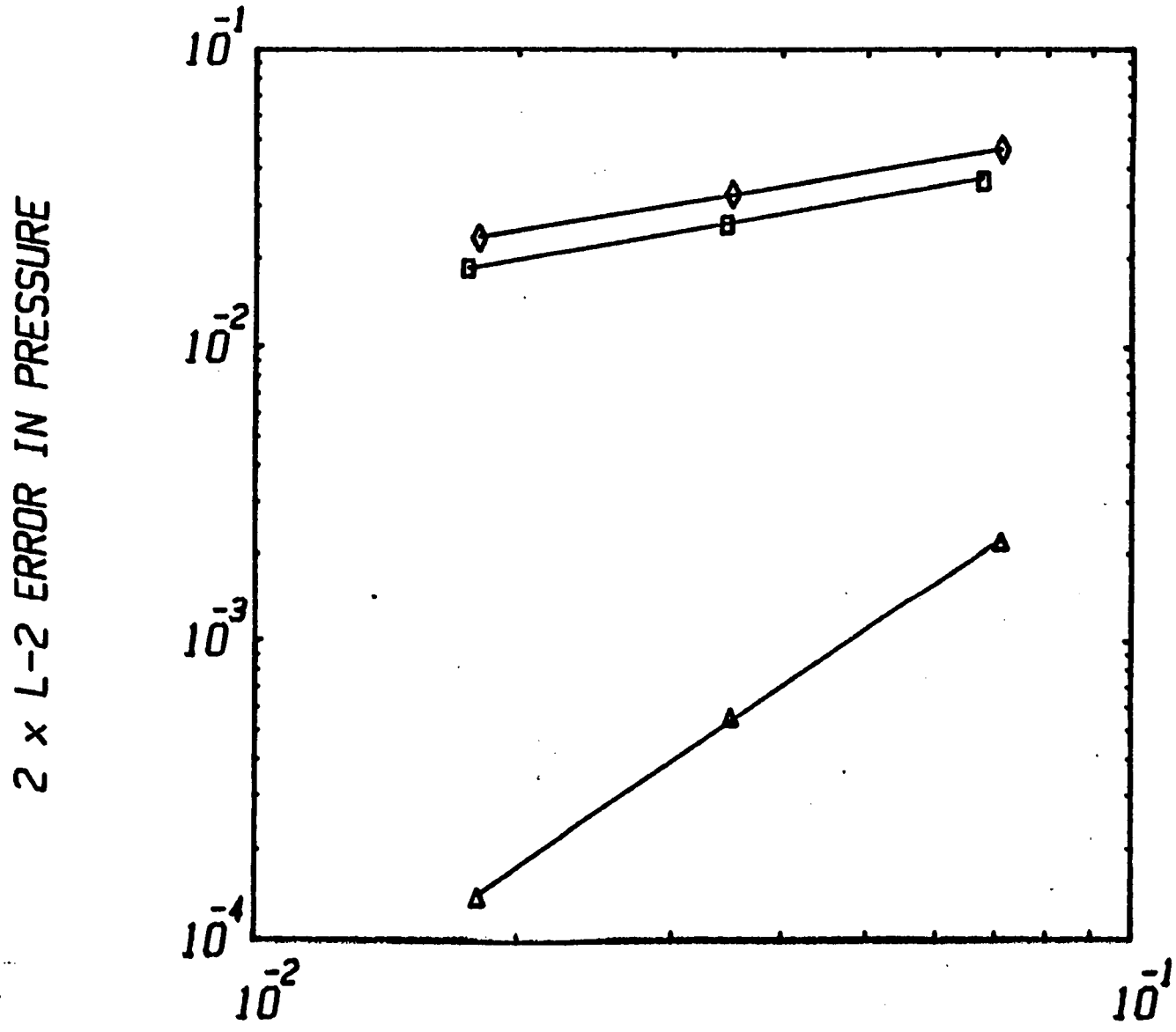

Figure 7.

L^2 error in the uniform duct case. $-\Delta-$ discontinuous elements, optimal convergence (slope =2). $-\square-$, $-\Diamond-$, suboptimal convergence (slope =1) when continuous pressures are imposed or elements bisect boundary of the flow discontinuity.

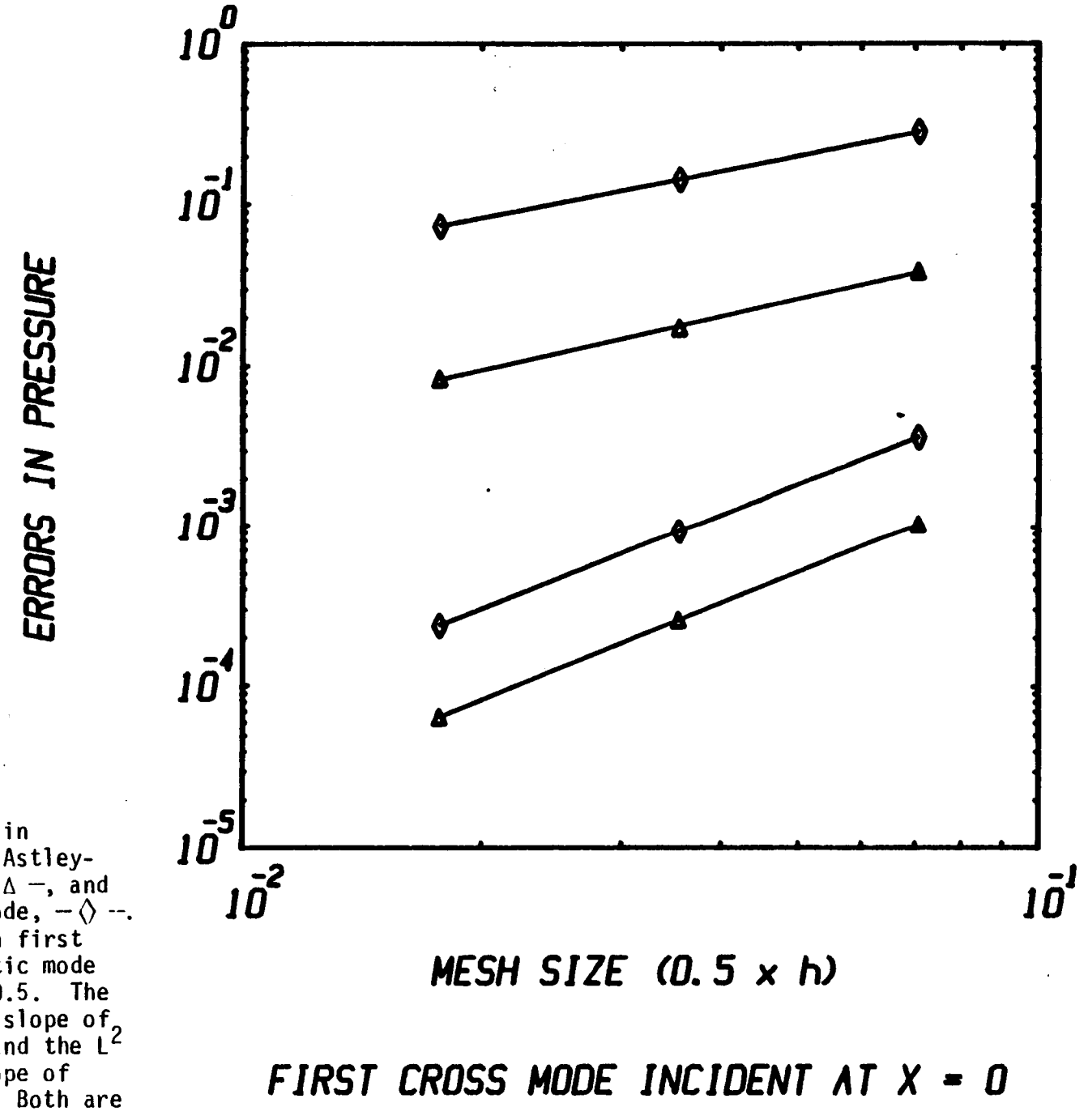

Figure 8.

H^1 and L^2 errors in velocity for the Astley-Eversman code, $-\Delta-$, and the Abrahamson code, $-\langle\rangle$ --. Uniform duct with first transverse acoustic mode incident. U = -0.5. The H^1 errors have a slope of approximately 1 and the L^2 errors have a slope of approximately 2. Both are suboptimal.

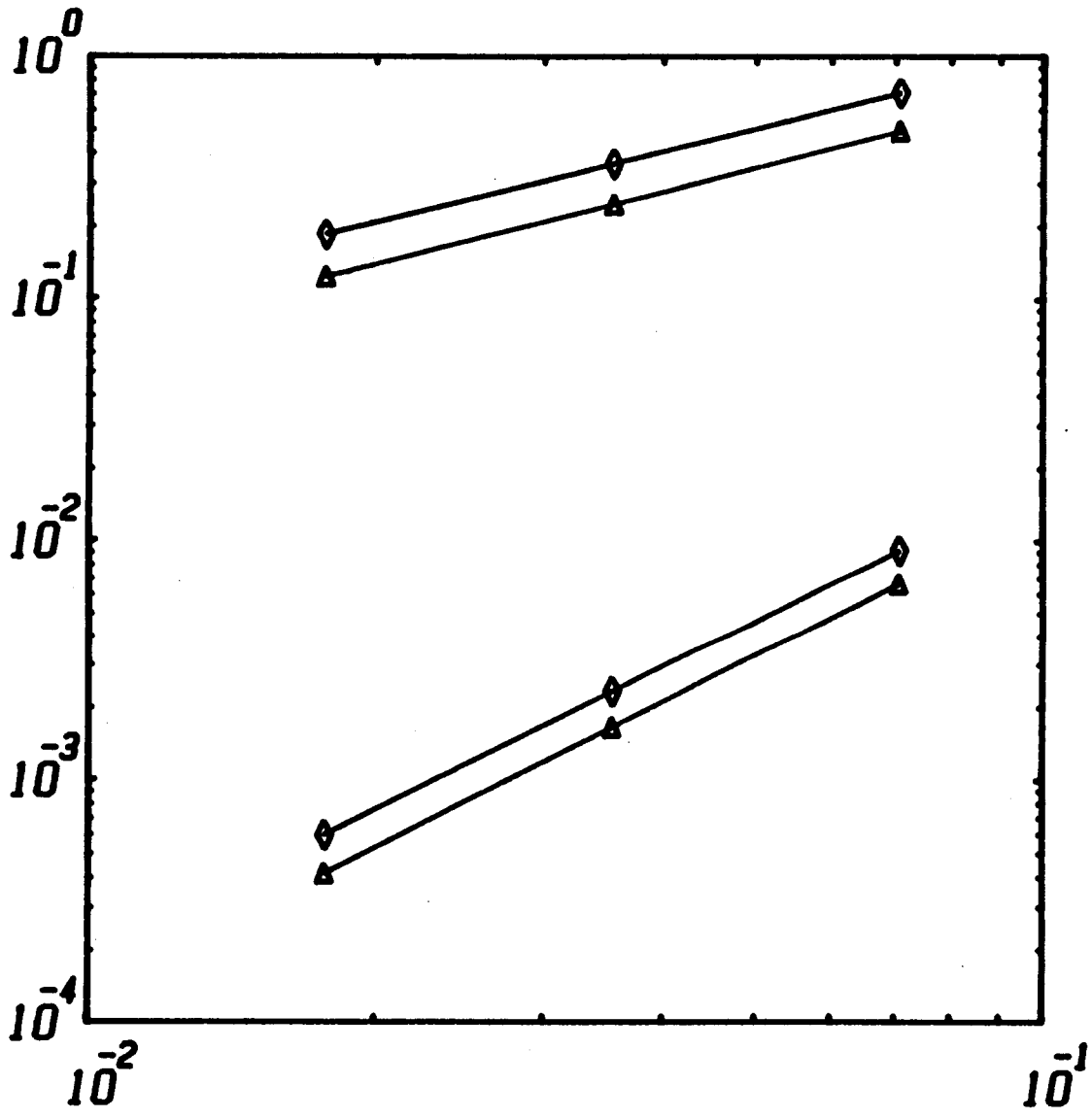

Figure 9.

H^1 and L^2 errors in pressure for the Astley-Eversman code, $-\Delta-$, and the Abrahamson code, $-\langle\rangle-$. Uniform duct with first transverse acoustic mode incident. U = -0.5. The H^1 errors have a slope of approximately 1 and the L^2 errors have a slope of approximately 2. Both are suboptimal.

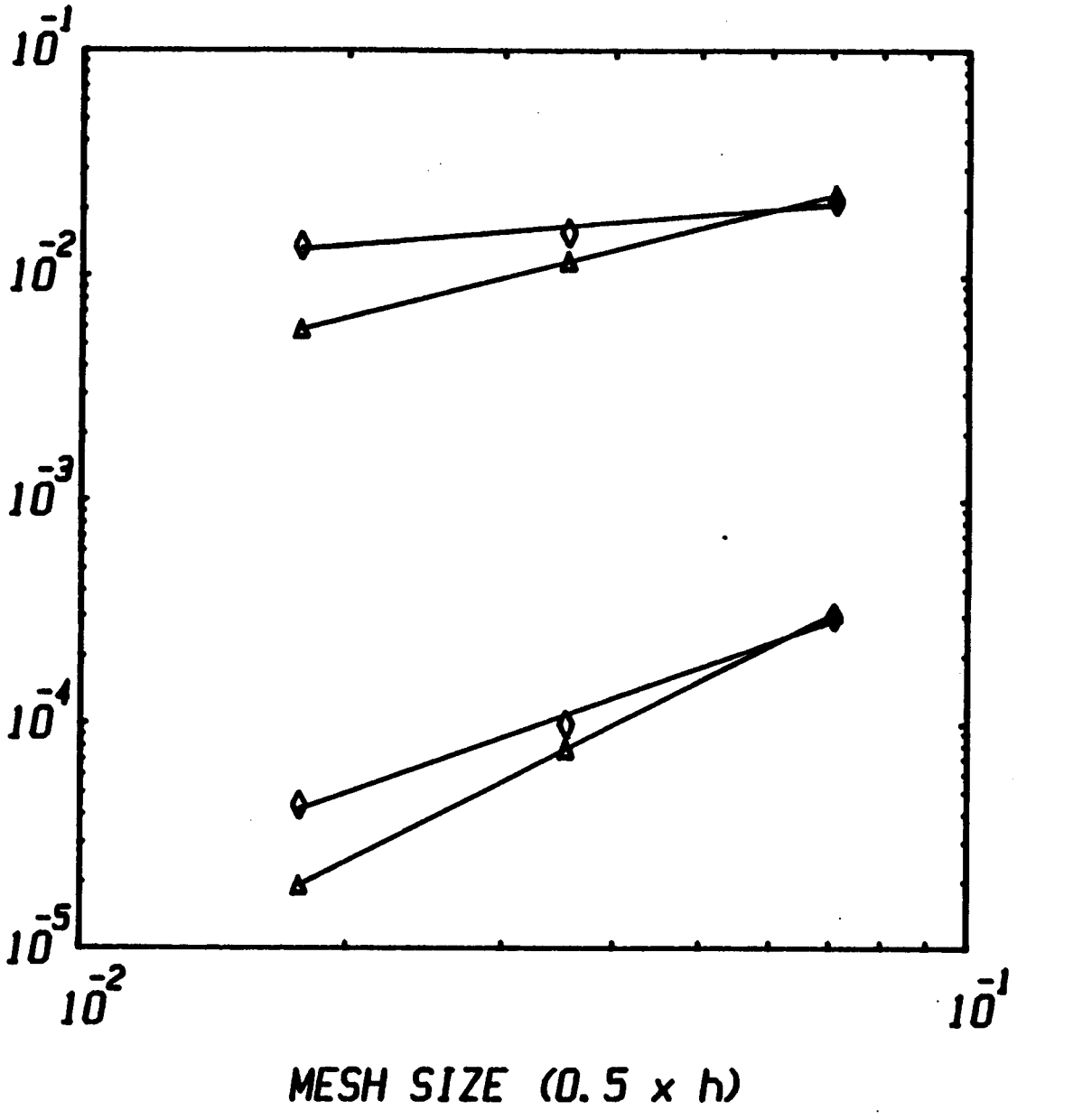

Figure 10.

H^1 and L^2 errors in velocity for the Astley-Eversman code, $-\Delta-$, and the Abrahamson code, $-\Diamond-$. Uniform duct with first hydrodynamic mode incident. U = -0.5. For the A-E code the H^1 error slope is 1.5 and the L^2 error slope is 2.3. For the Abrahamson code the H^1 error slope is 1.0 and the L^2 error slope is 2.0

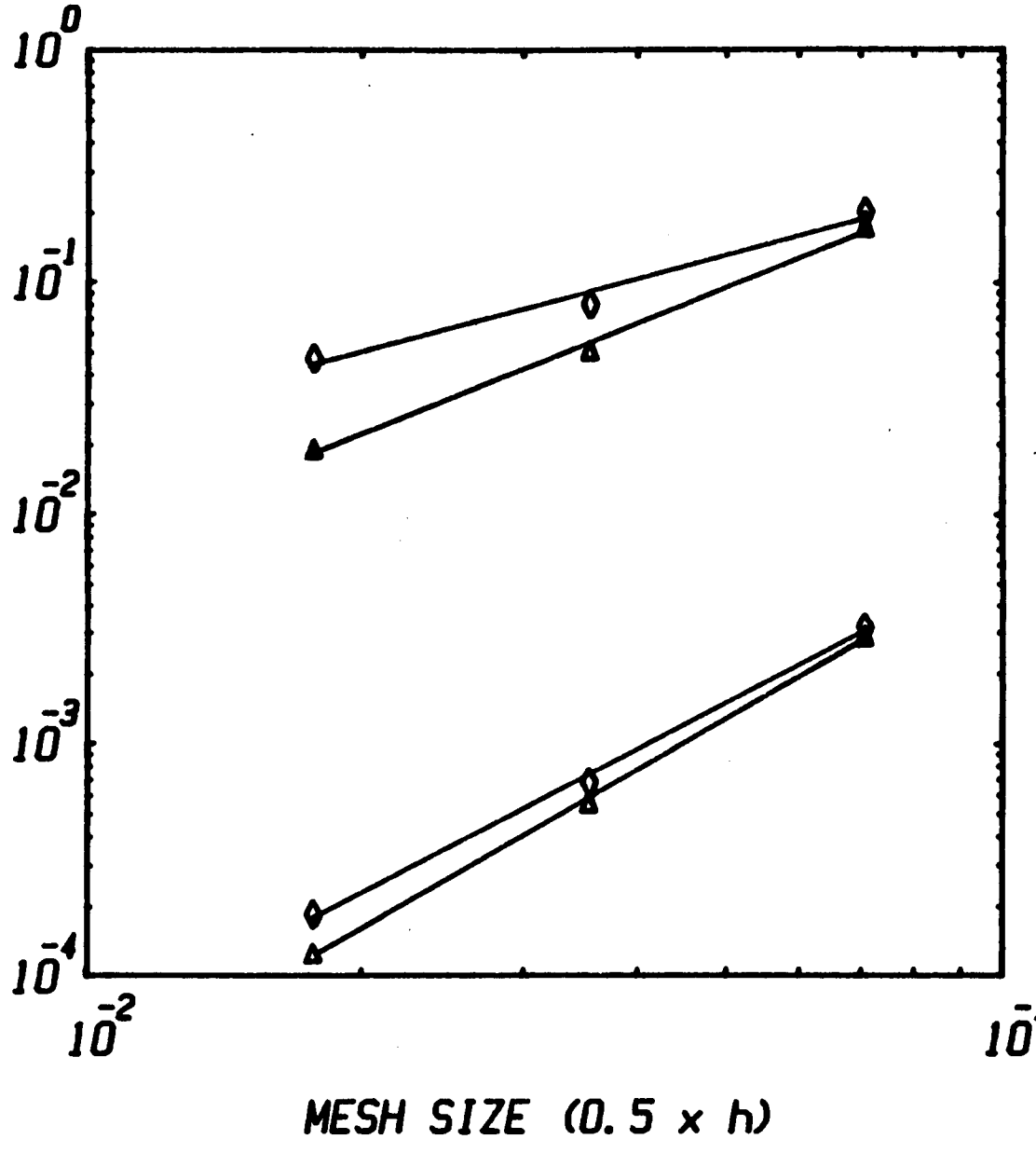

Figure 11.

H^1 and L^2 errors in pressure for the Astley-Eversman code, $-\Delta-$, and the Abrahamson code, $-\Diamond-$. Uniform duct with first hydrodynamic mode incident. U = -0.5. For the A-E code the H^1 error slope is 1.0 and the L^2 error slope is 2.0. For the Abrahamson code the H^1 error slope is 0.3 and the L^2 error slope is 1.4.

2. Non-Uniform Duct Results

The problems with convergence reported by Abrahamson [7] were encountered with the non uniform mean flows that are usually encountered with variable geometries. In order to compare the performance of the codes in such a situation a quartic half duct was chosen as a test problem. The quartic duct under consideration was symmetric about the throat and had terminations that were uniform ducts. The throat to exit area ratio was chosen as 0.5 and the duct length and termination height were both set to 1.0. Three mean flow cases were considered:

Case (a) The simplest mean flow was constructed by solving the one dimensional nozzle equations to yield an x component of mean flow velocity, density and speed of sound. The y component of velocity at the upper wall was chosen so that the flow would be tangential, elsewhere it varied linearly from zero on the center line to its maximum value on the upper wall. The inlet/outlet Mach. number was chosen to be 0.3 yielding a Mach. number of 0.86 on the duct centerline at the throat.

Case (b) The next mean flow was constructed by modifying the flow described in part (a) above to give a boundary layer at the throat. To create the boundary layer a weight (w) was calculated according to

$$w(x,y) = \sin\left[\frac{\pi}{2}\left(1 - \frac{y}{Y(x)}\right)^{\frac{4}{\ell^2} x\,(\ell - x)}\right]$$

where

$Y(x)$ is the duct width at x.

The modified velocity field was then the product of the velocity field given in part (a) and the weight w. At the throat this weight gives a sinusoidal boundary layer. The density and speed of sound were not adjusted.

Case (c) The third mean flow was constructed like the one in (b) above except that a much steeper boundary layer was chosen. A one-seventh boundary layer approximation, similar to the empirical relation observed in pipes, was used. The weight (w) chosen to yield such a layer is given by,

$$w(x,y) = \left[1 - \frac{y}{Y(x)} \frac{4}{\ell^2} x\ (\ell - x)\right]^{1/7}$$

The mean flow, for all three cases, was evaluated at the nodal values of the finite elements, and the element interpolation functions were used to determine the flow within an element. Eight noded isoparametric elements were used for all cases. Case (c) has very steep gradients so the element interpolation functions would not approximate these gradients very well on a coarse mesh, however, since this is typical of what happens in practice we did not make any attempt to correct this problem. The mean flow for case (c) has a singularity in its derivatives at the throat so the integrals defined for the Astley and Abrahamson weak problems may not be continuous.

Since the mean flow varies rapidly near the throat and at the upper wall, meshes were chosen that had a higher density of elements in these regions. The meshes were constructed using the following transformation for the nodal spacing in the x direction,

$$x(\xi) = \frac{1}{2}\left[1 + \frac{\xi(1+x)^2)}{1+x}\right], \quad -1 \leq \xi \leq 1 \quad x = 1.0$$

Equal increments of ξ were used to yield nodal x values. The following transformation was used for the nodal spacing across the duct,

$$y(\eta) = Y(x) \cdot \eta\left[\frac{(2x+1) - \eta\chi}{x+1}\right], \quad 0 \leq \eta \leq 1 \quad x = 1.5$$

where

Y(x) is the duct width at x.

Again equal increments of η were used to yield the nodal y values at each axial location. Along straight sides the midside nodes were always placed in the middle. A typical mesh with 5 elements across the duct and 10 elements along the duct (a 5 x 10 grid) is shown in figure 12. Three meshes, 5 x 10, 10 x 20 and 20 x 40 elements, were utilized for each of the three cases (a-c) described above. The frequency (ω) was set to 2.0 and the problem of a plane wave incident at x=0 ($a_0^+ = 1.0$) was selected. For this problem the meshes described above would be considered very fine since they have many elements per wave length. With realistic geometries and frequencies meshes with a similar number of elements per wave length would probably exceed the capabilities of most computers.

As no exact solution exists for the non uniform duct problem a comparison of plots of pressure amplitude contours is made. It is expected that if the contours are smooth where the mean flow is smooth, and if the contour pattern only changes slightly as the mesh is refined, the solution is converging. When appropriate, plots of the pressure are presented for comparison of the schemes. For the finest grid,

calculations were made of the L^2 difference between the pressure given by the potential flow code and the pressure given by the other two algorithms.

Figures (13a-c) show the pressure contours for case (a) given by each of the three codes with the 20 x 40 mesh. Using the criteria discussed above, it appears as if the potential flow code and Astley's algorithm are converging, however the plot given by Abrahamson's algorithm is not particularly smooth and it is difficult to conclude anything. One conspicuous difference between the potential flow code and the other two algorithms is the apparent rate of convergence (cf. the uniform duct solutions). Figures (14a-c) show the pressure contour plots for each of the three algorithms given with the coarsest (5 x 10) mesh. Figure (14a) shows that the potential flow code contours are qualitatively the same as those for the finer mesh, figure (13a), however, the contours for the other two algorithms show the presence of large wiggles which almost obscure any pattern present.

Figures (15a-c) show the pressure contours given by the three algorithms for case (b) on the finest mesh. Case (b) exhibits the trends discussed in case (a) above and, if anything, to a greater degree. Comparing the contour patterns given by the potential code and Astley's algorithm shows a difference in the pressure near the upper wall. Figures (16a-c) show the wall pressure plots corresponding to the three contour plots given in figures (15a-c). It is apparent that the rotational codes develop a different pressure profile at the upper wall near the throat. Another difference between the rotational and irrotational codes is the level of the solution. This is indicated

qualitatively by the peak pressures in the throat given in figures 15, and quantitatively by the L^2 norms of the solutions given in figure 17. Figure 17 contains the norms of the solutions for each of the three cases and the L^2 difference between the potential flow pressures and the pressures given by the rotational codes for the finest grid.

Figures (18a-c) show the pressure contour plots given by each of the three codes for case (c). Inspection of these plots shows that Abrahamson's algorithm almost certainly is not converging and that the potential flow solution almost certainly is. The results given by Astley's algorithm are inconclusive and are very similar to those of Abrahamson's algorithm for cases (a) and (b). Figure (19a-c) show plots of the pressure along the lines x=0, x=0.5 and x=1.0 given by each of the algorithms on the finest mesh. The pressure given by the velocity potential code at the throat contains a discontinuity. The pressure at the throat given by Astley's algorithm is similar but it is reminiscent of the pressures shown in figures (5) and (6) where continuous pressures were used to model a pressure jump that was modeled much better by the discontinuous elements. The pressures given by Abrahamson's code at each of the three axial locations contain tremendous wiggles.

Figure 17 tabulates the L^2 pressure norms given by each algorithm for cases (a-c) on each of the meshes and the L^2 difference between the rotational and irrotational pressures with the finest mesh. It is apparent that the pressure is consistently larger for the potential flow code than the rotational flow pressure and it appears that if the Abrahamson and Astley algorithms converge, the pressure is similar. The L^2 difference

between the pressures given by the irrotational and rotational algorithms was greatest for case (b) where they differed by about 30%. The difference for cases (a) and (b) were approximately 10% and 15% respectively.

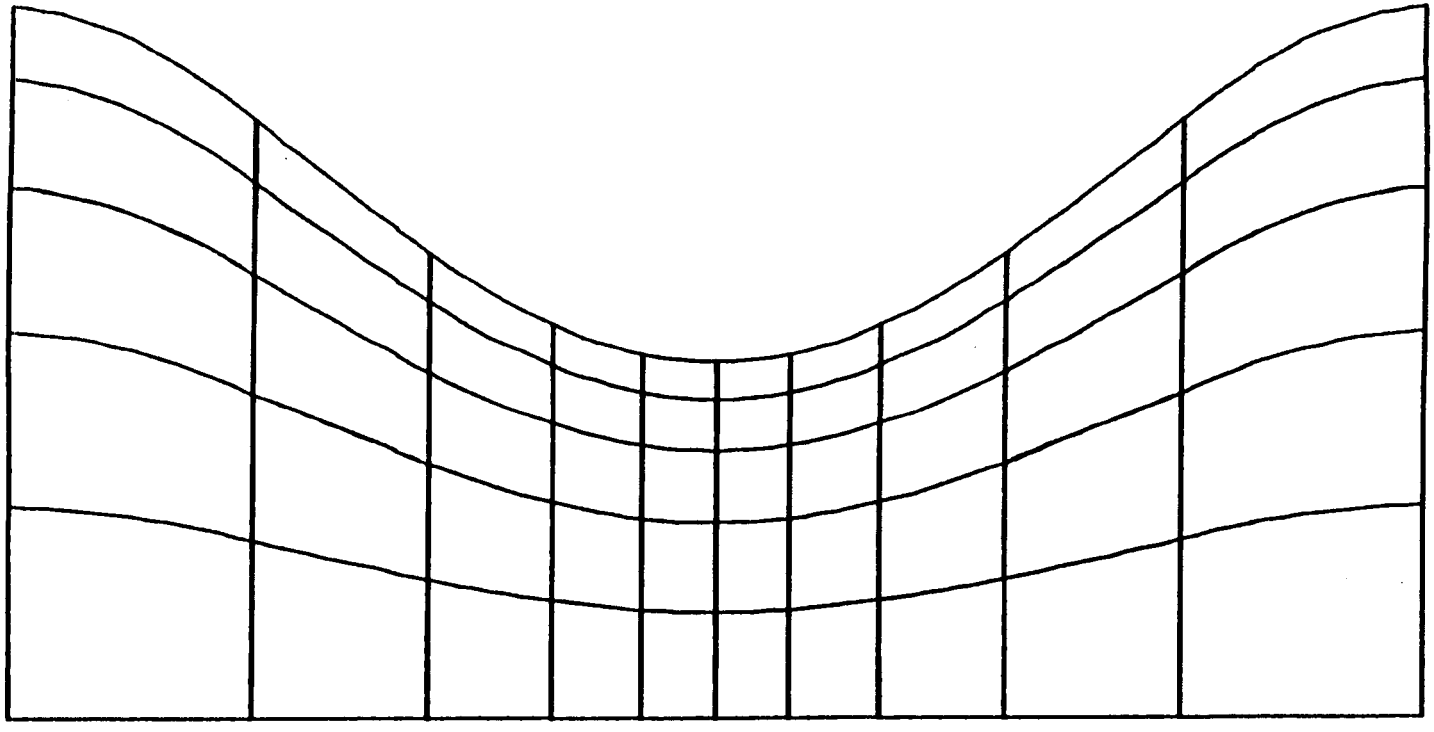

Figure 12. Quartic duct profile used in nonuniform duct convergence studies. Shown here is the coarsest mesh, 5 x 10.

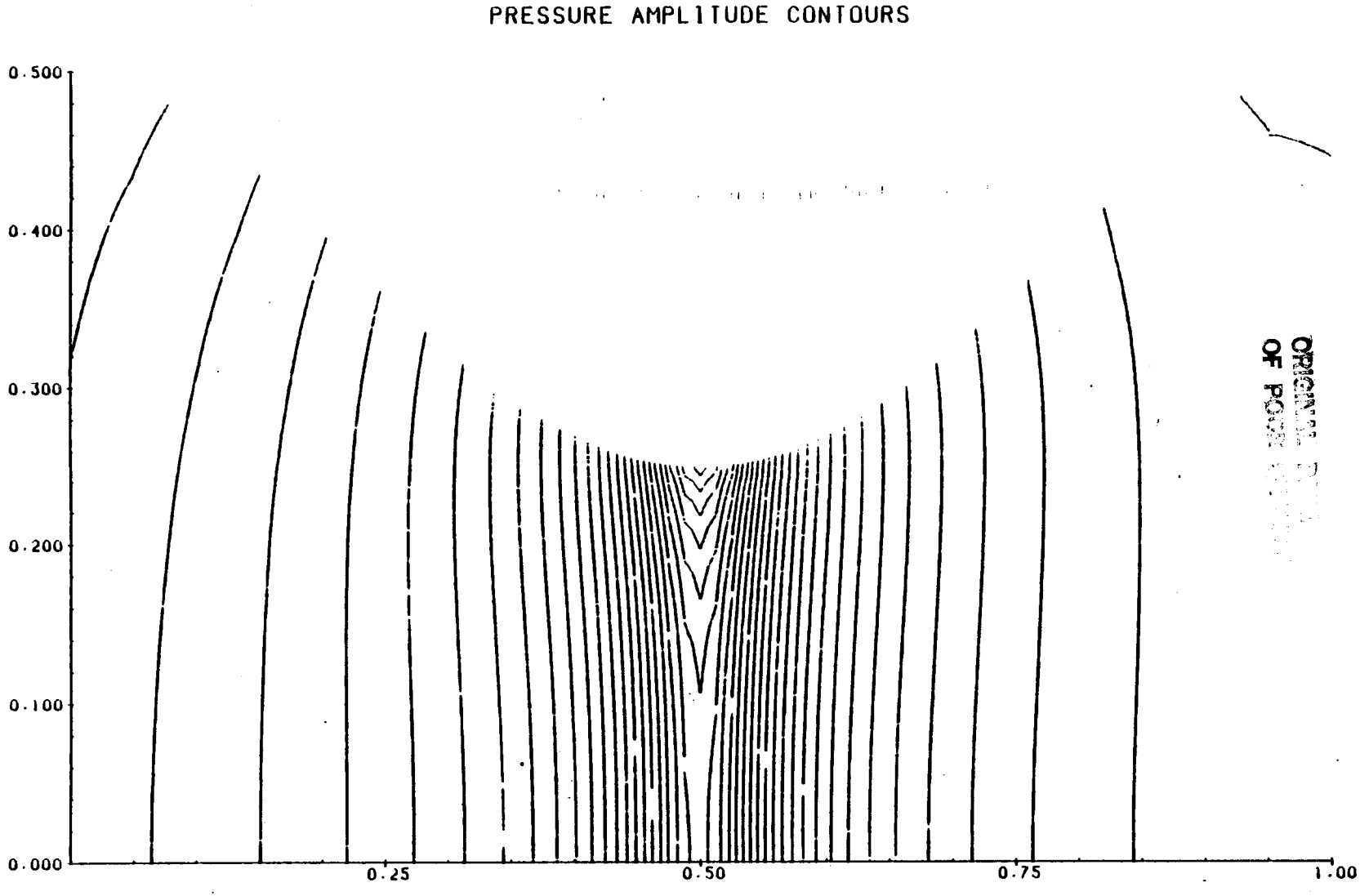

Figure 13(a). Pressure contours for nonuniform duct case (a). Velocity potential formulation. 20 x 40 mesh.

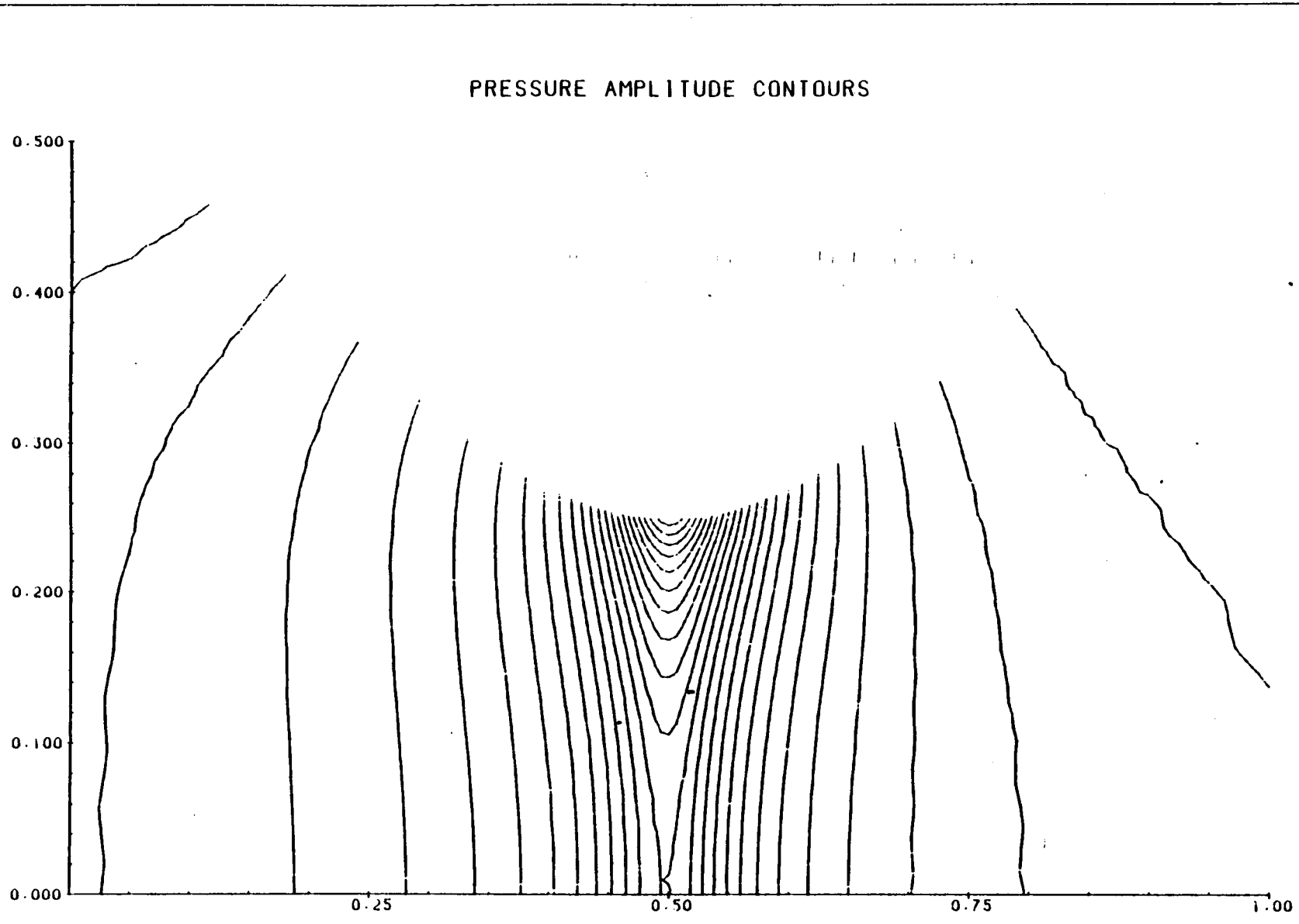

Figure 13(b). Pressure contours for nonuniform duct case (a). Astley-Eversman formulation. 20 x 40 mesh.

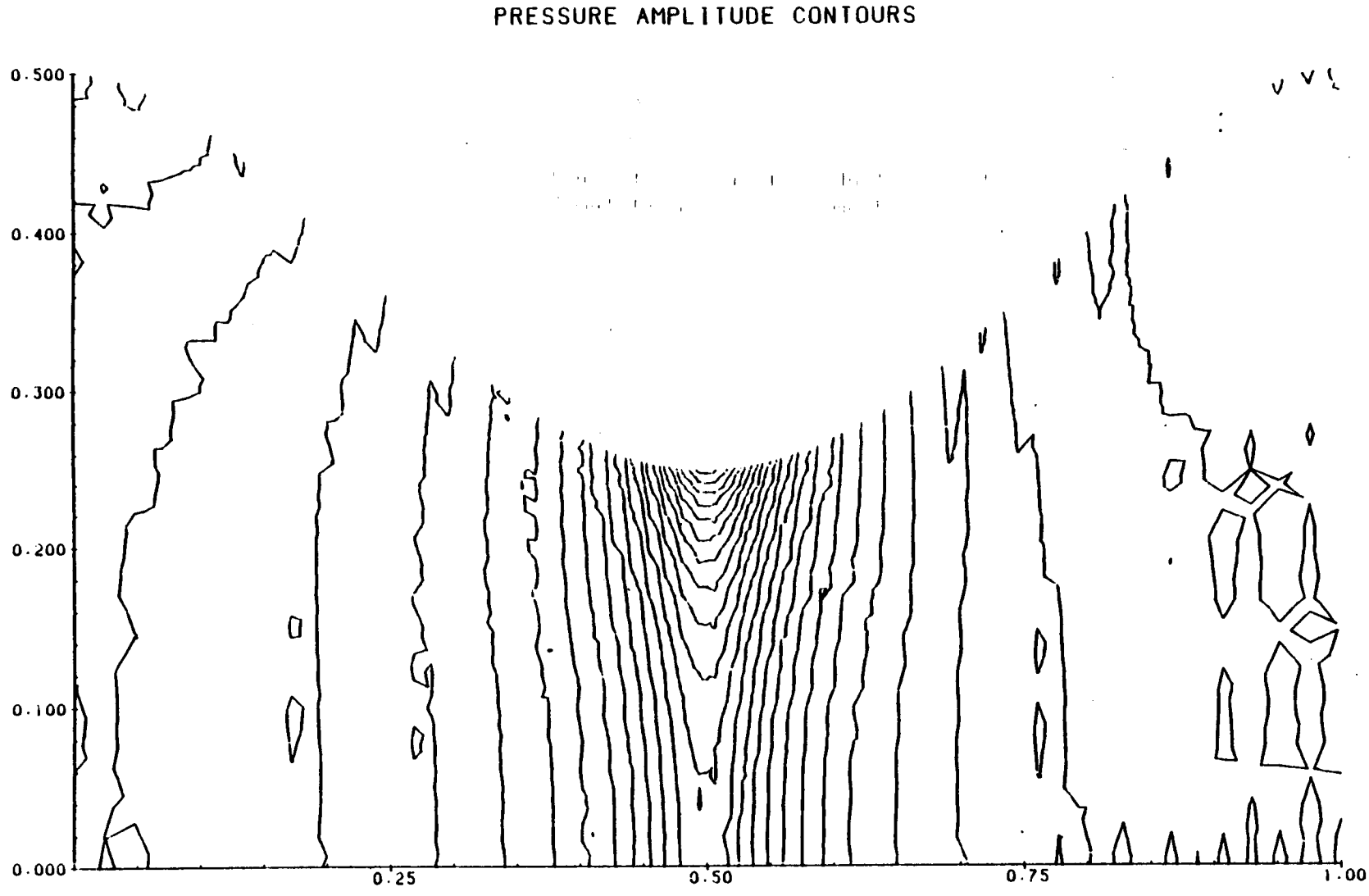

Figure 13(c). Pressure contours for nonuniform duct case (c). Abrahamson formulation. 20 x 40 mesh.

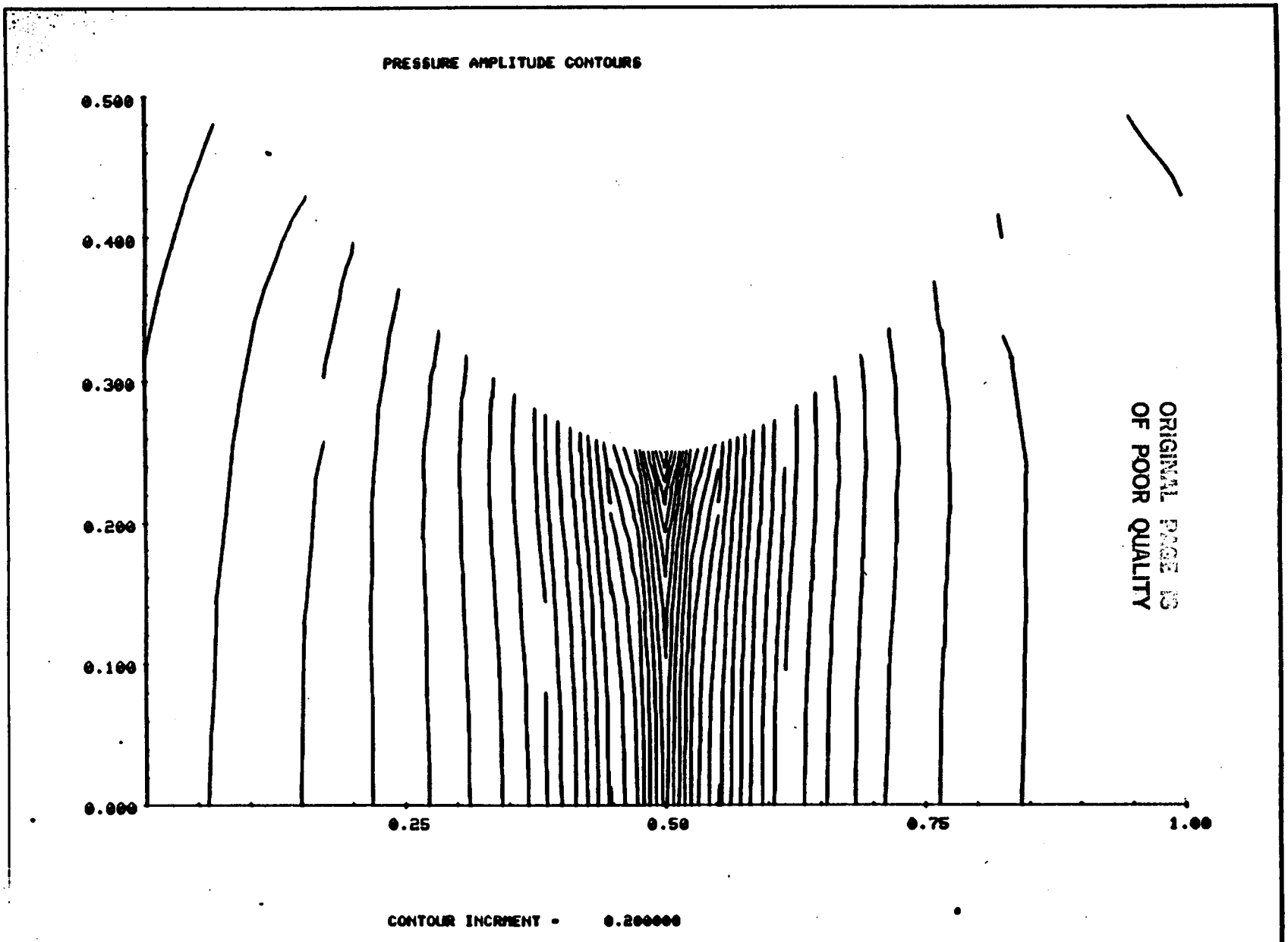

Figure 14(a). Pressure contours for nonuniform duct case (a). Velocity potential formulation. 5 x 10 mesh.

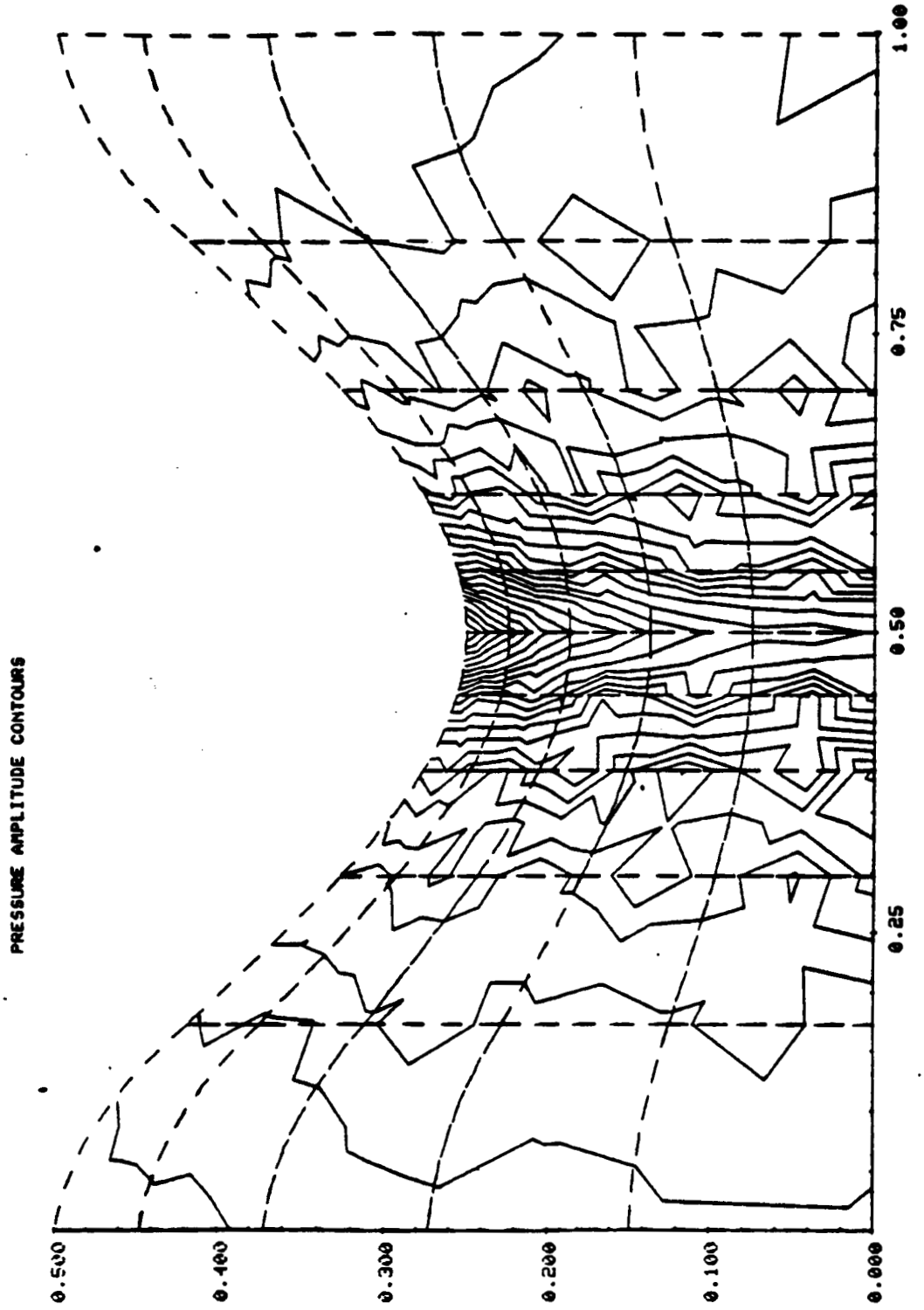

Figure 14(b). Pressure contours for nonuniform duct case (a). Astley-Eversman formulation. 5 x 10 mesh.

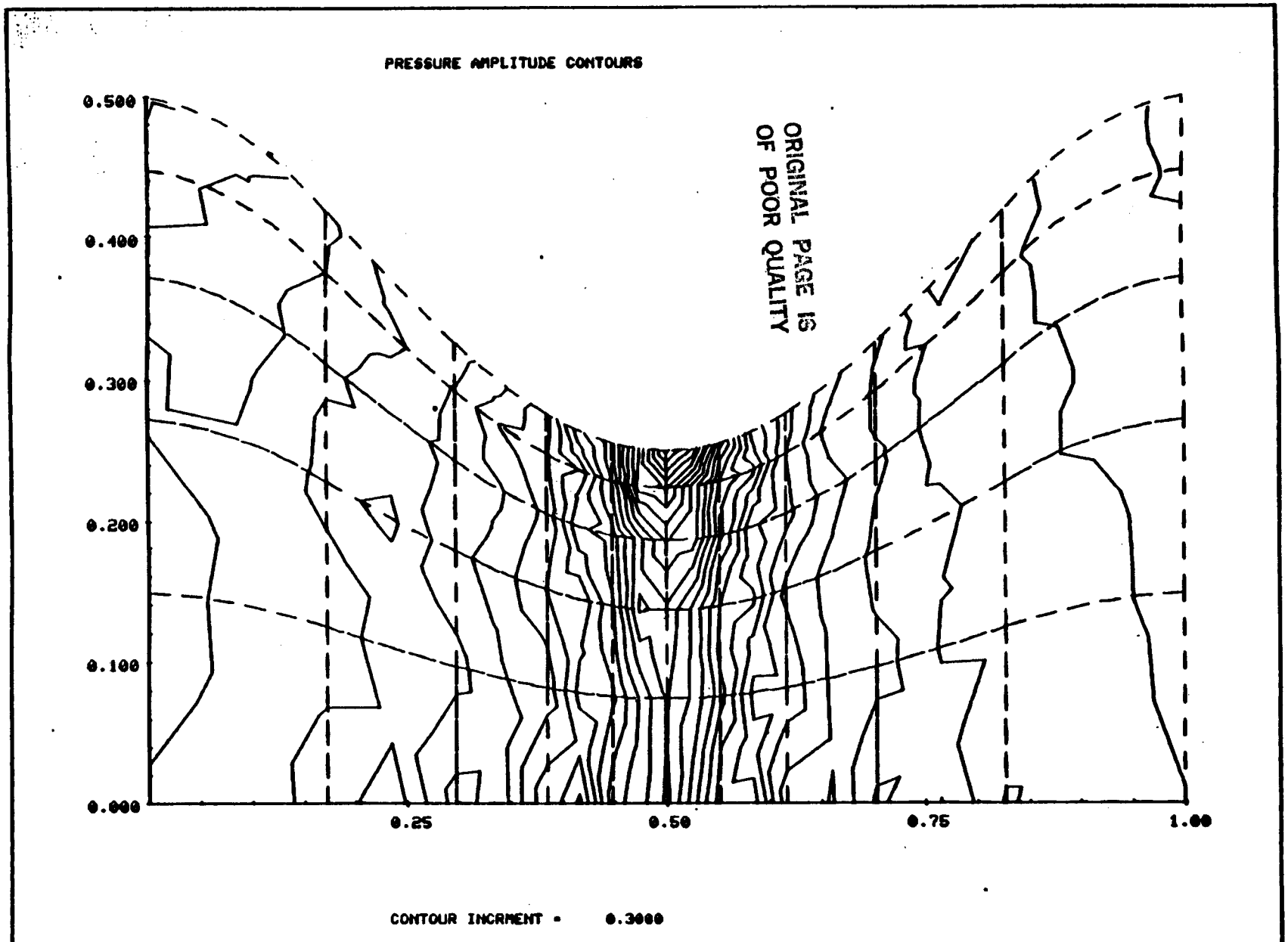

Figure 14(c). Pressure contours for nonuniform duct case (a). Abrahamson formulation. 5 x 10 mesh.

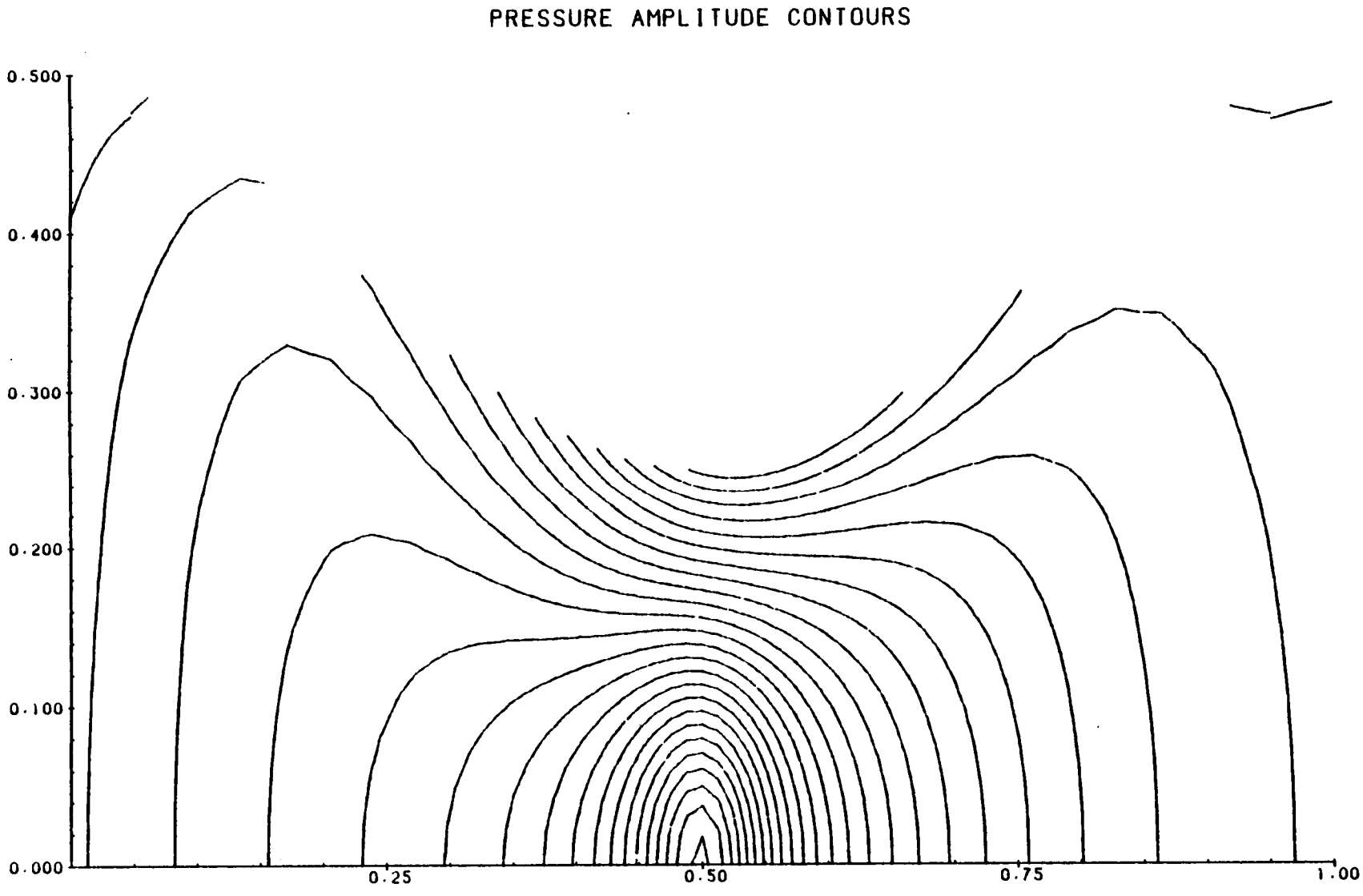

Figure 15(a). Pressure controus for nonuniform duct case (b). Velocity potential formulation. 20 x 40 mesh.

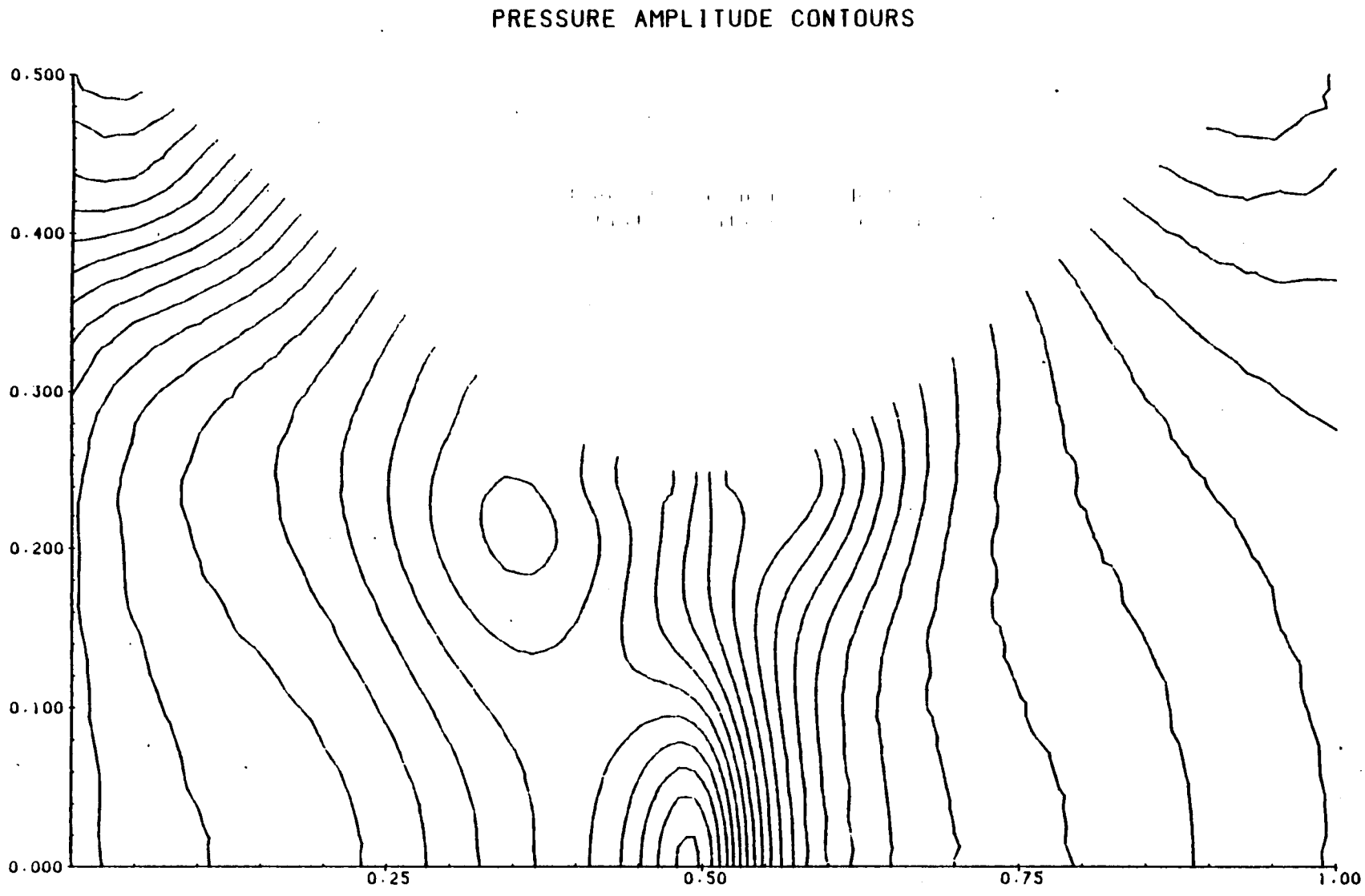

Figure 15(b). Pressure contours for nonuniform duct case (b). Astley-Eversman formulation. 20 x 40 mesh.

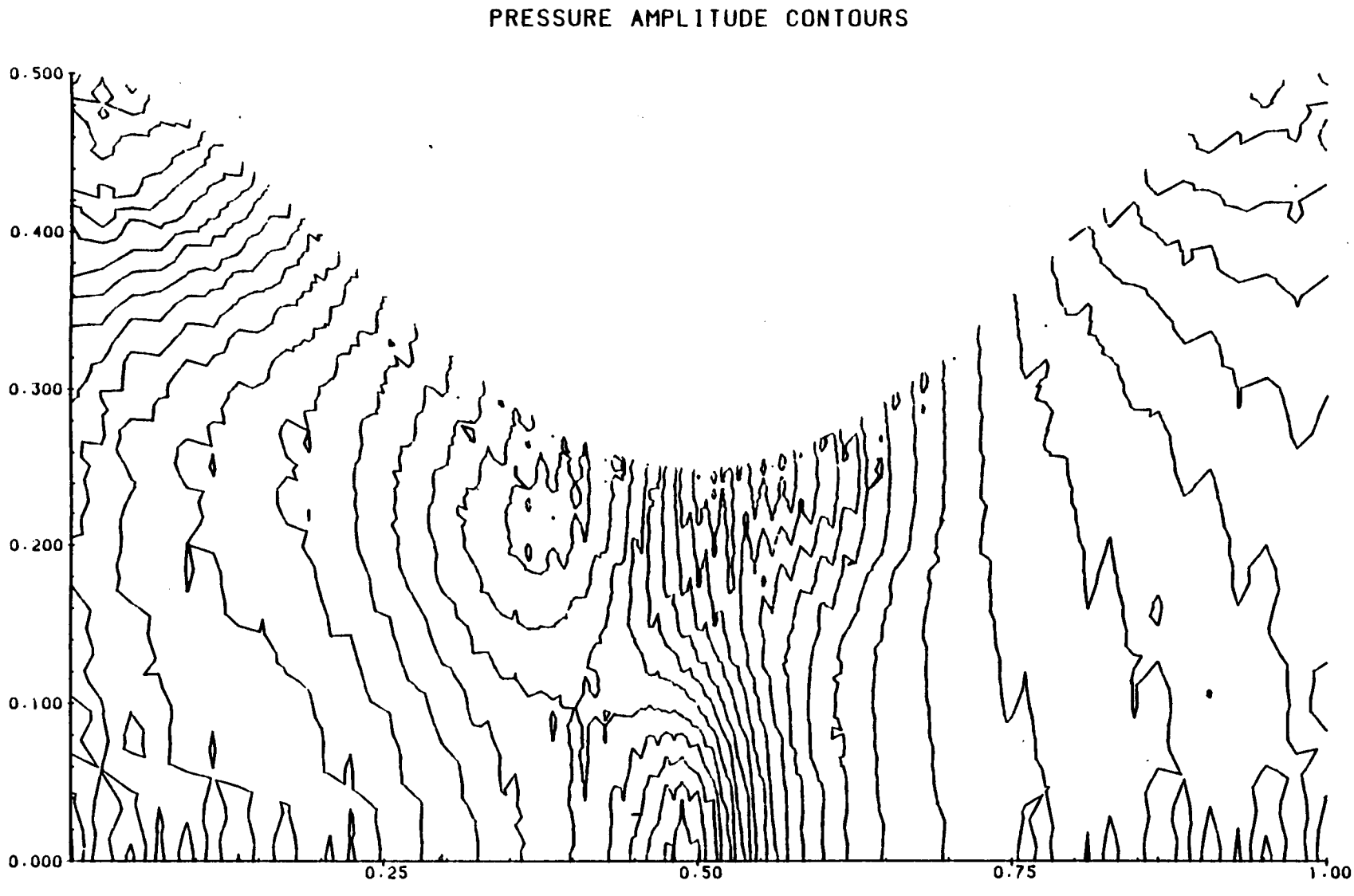

Figure 15(c). Pressure contours for nonuniform duct case (b). Abrahamson formulation. 20 x 40 mesh.

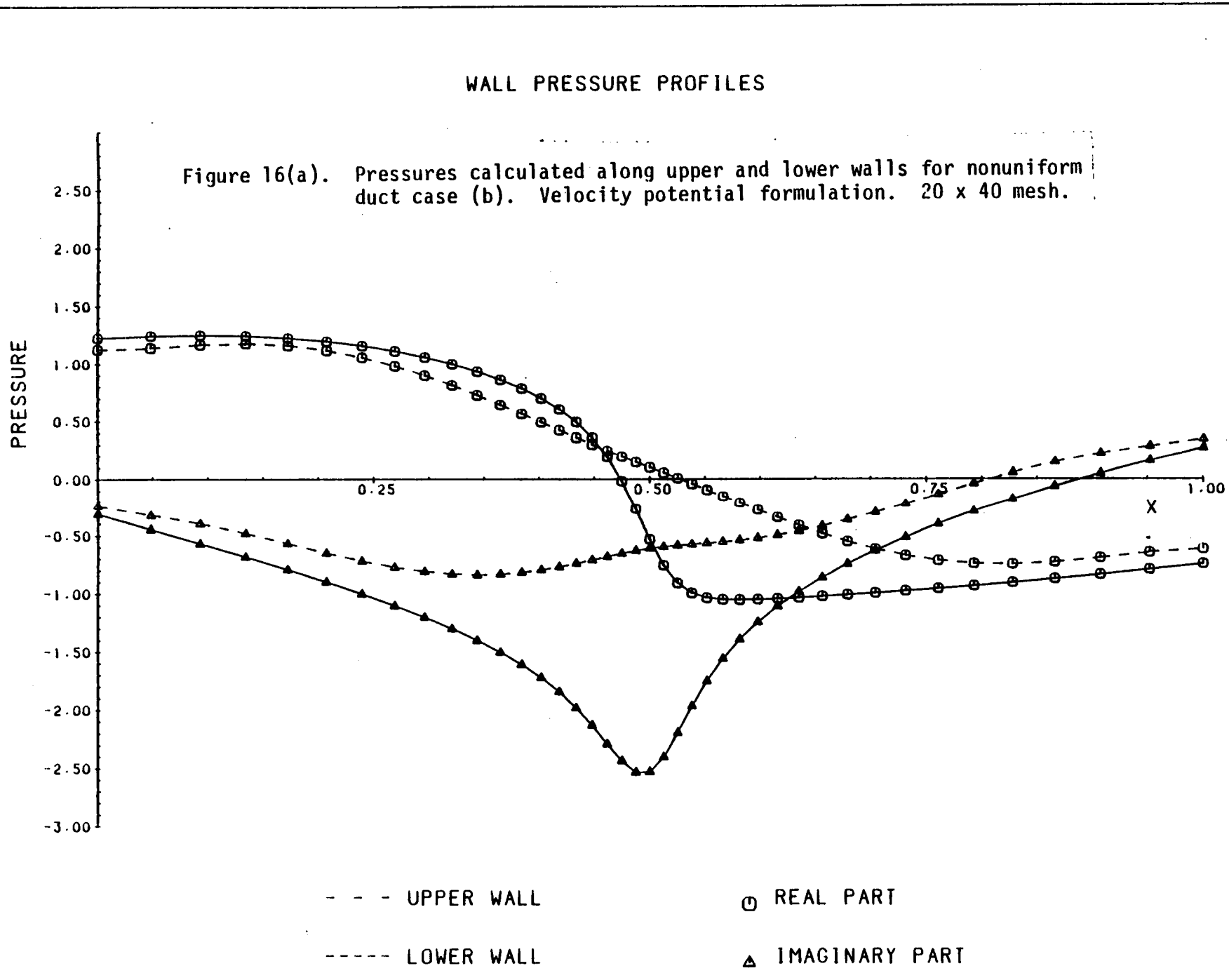

Figure 16(a). Pressures calculated along upper and lower walls for nonuniform duct case (b). Velocity potential formulation. 20 x 40 mesh.

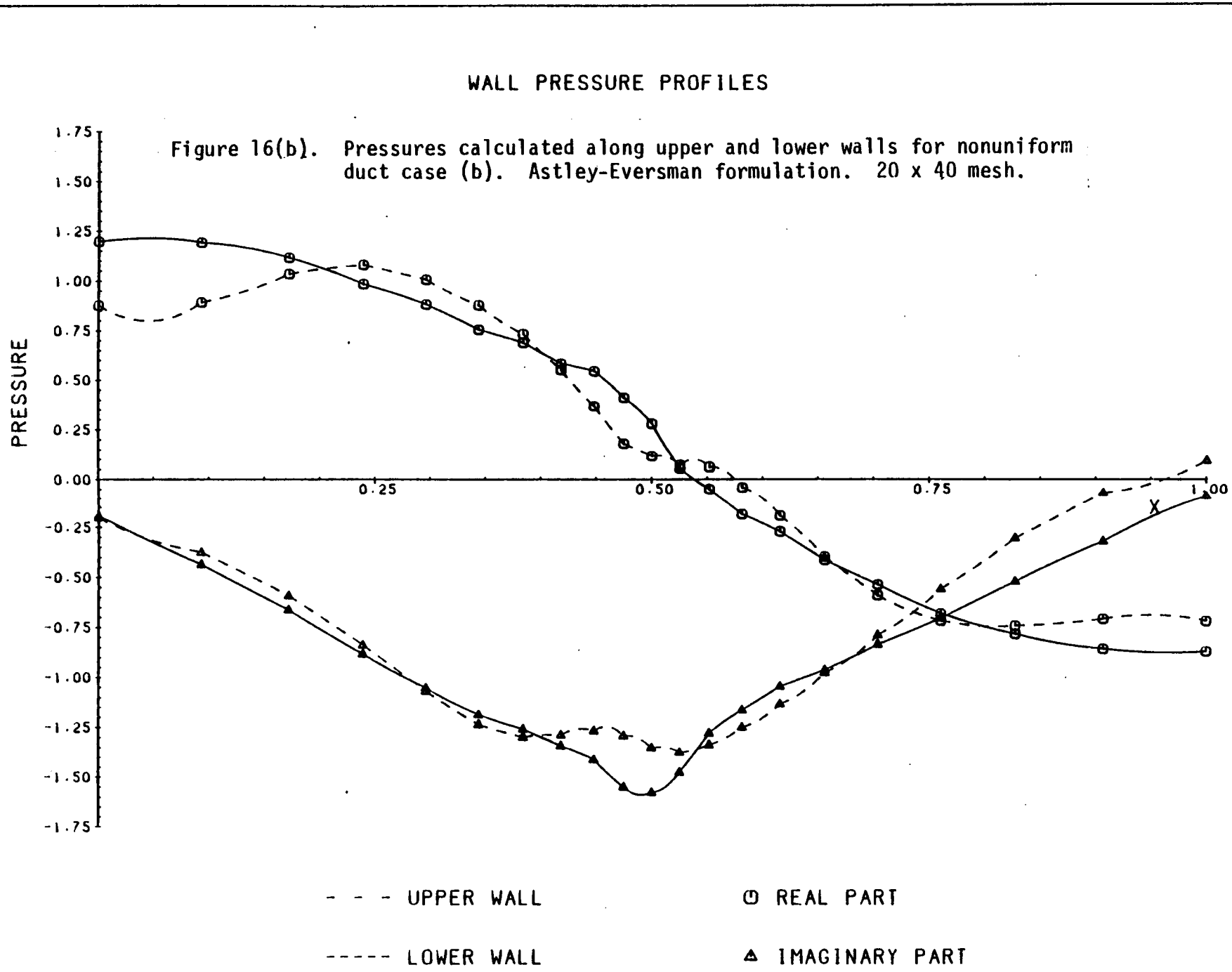

Figure 16(b). Pressures calculated along upper and lower walls for nonuniform duct case (b). Astley-Eversman formulation. 20 x 40 mesh.

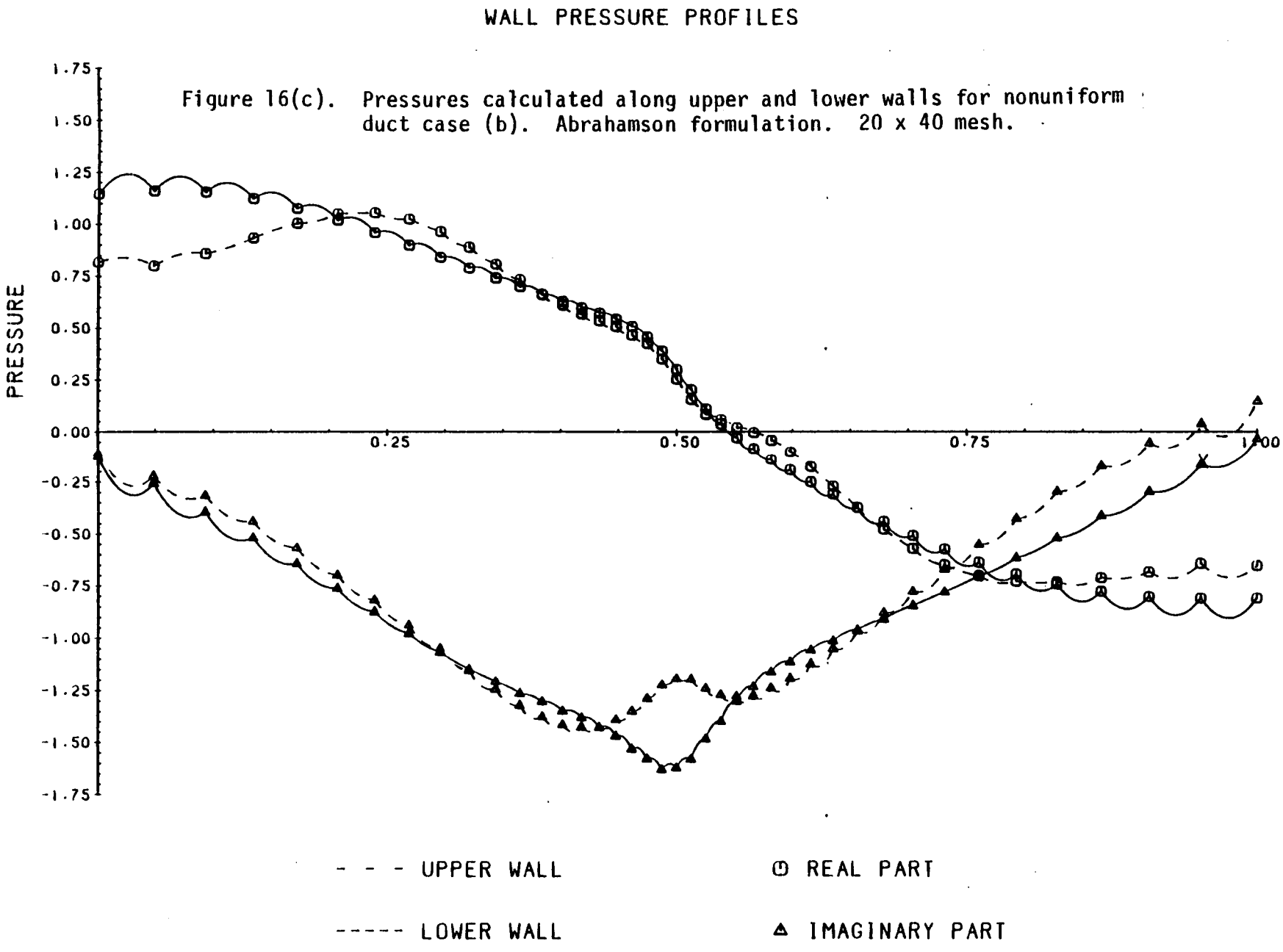

Figure 16(c). Pressures calculated along upper and lower walls for nonuniform duct case (b). Abrahamson formulation. 20 x 40 mesh.

Mesh	CASE (a)			CASE (b)			CASE (c)		
	Pot. Flow	Astley	Abrahamson	Pot. Flow	Astley	Abrahamson	Pot. Flow	Astley	Abrahamson
5 x 10	1.220	1.221	1.94	.755	.710	.683	.924	.916	.844
10 x 20	1.225	1.223	1.216	.755	.713	.709		.905	.901
20 x 40	1.225	1.223	1.209	.755	.713	.713	.923	.903	.912
*Difference		.098	.102		.246	.249		.134	.184

*The L^2 difference between the potential flow code pressures and those from the Astley and Abrahamson Algorithms on the 20 x 40 mesh.

Figure 17. L^2 Pressure Norms for the Non-Uniform Duct Examples

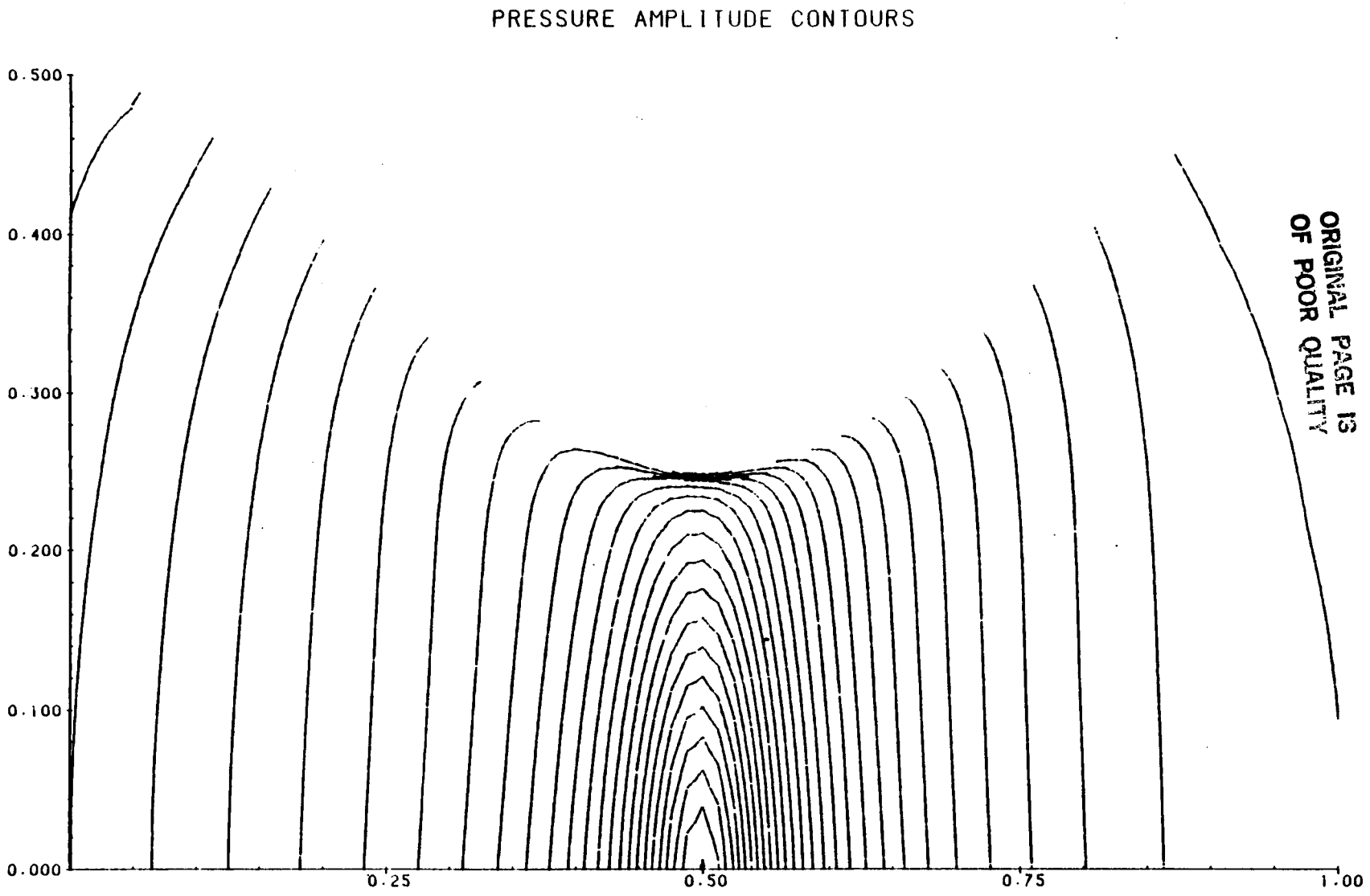

Figure 18(a). Pressure contours for nonuniform duct case (c). Velocity potential formulation. 20 x 40 mesh.

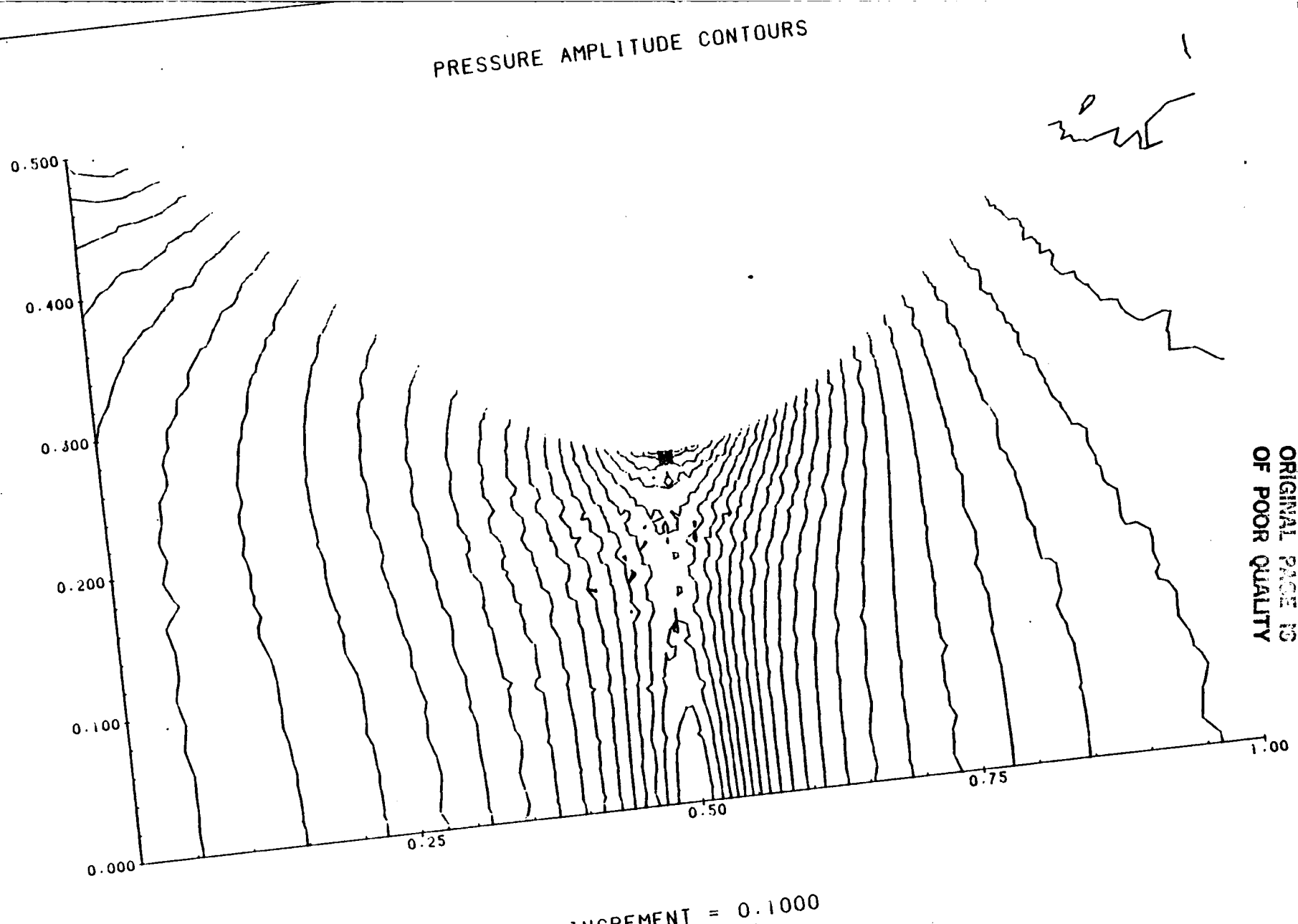

Figure 18(b). Pressure contours for nonuniform duct case (c). Astley-Eversman formulation. 20 x 40 mesh.

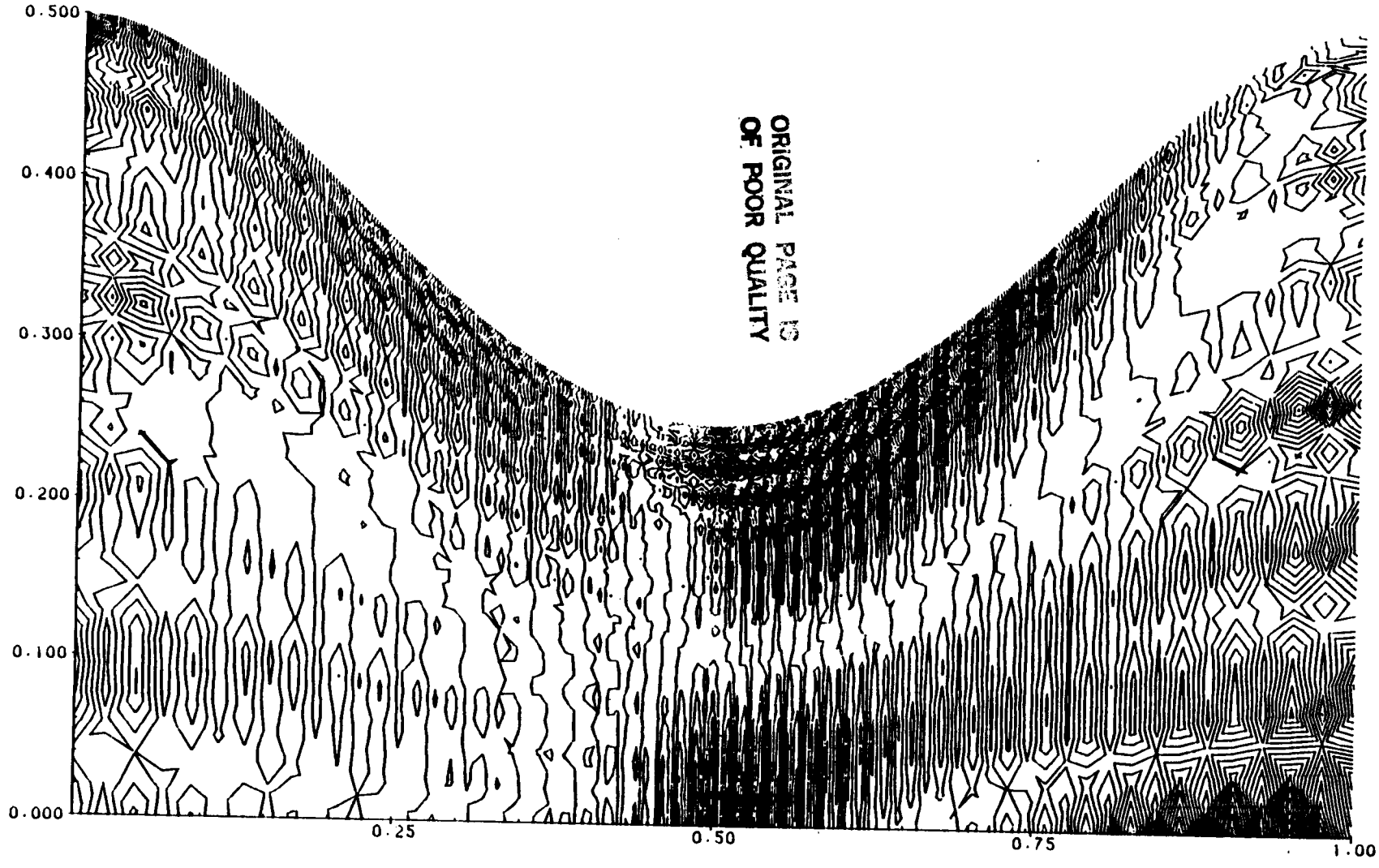

CONTOUR INCREMENT = 0.1000

Figure 18(c). Pressure contours for nonuniform duct case (c). Abrahamson formulation. 20 x 40 mesh.

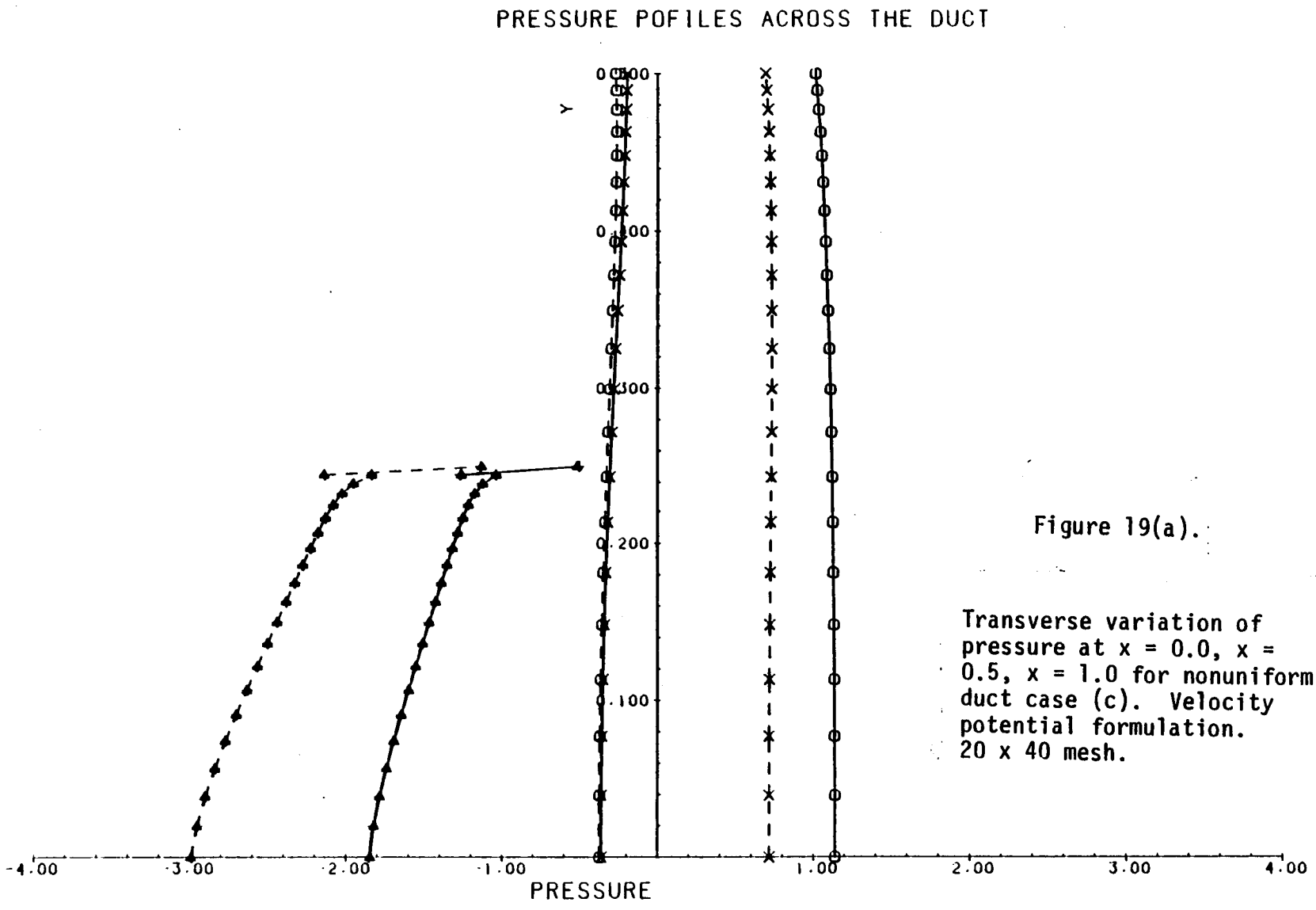

Figure 19(a).

Transverse variation of pressure at x = 0.0, x = 0.5, x = 1.0 for nonuniform duct case (c). Velocity potential formulation. 20 x 40 mesh.

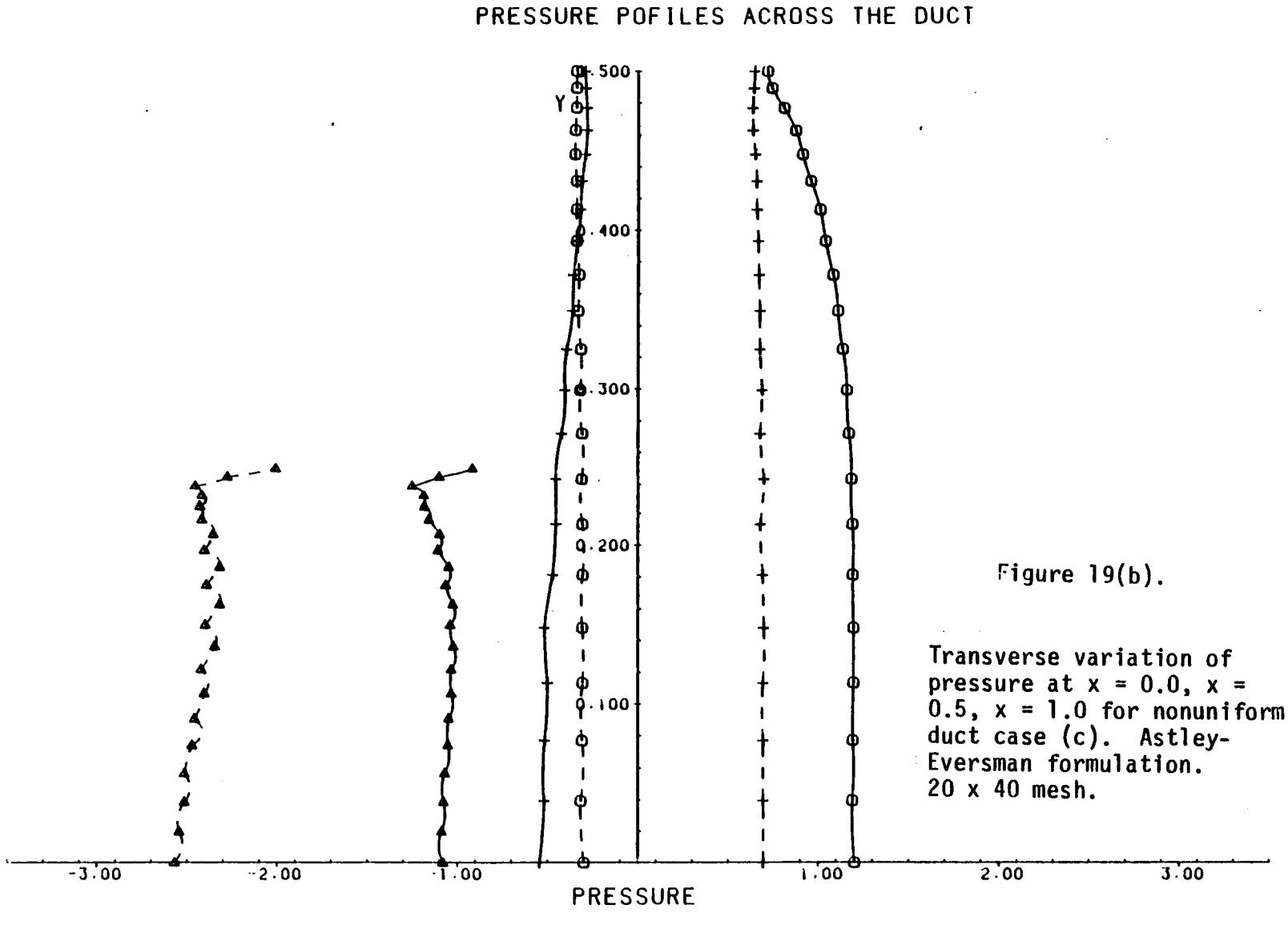

Figure 19(b).

Transverse variation of pressure at x = 0.0, x = 0.5, x = 1.0 for nonuniform duct case (c). Astley-Eversman formulation. 20 x 40 mesh.

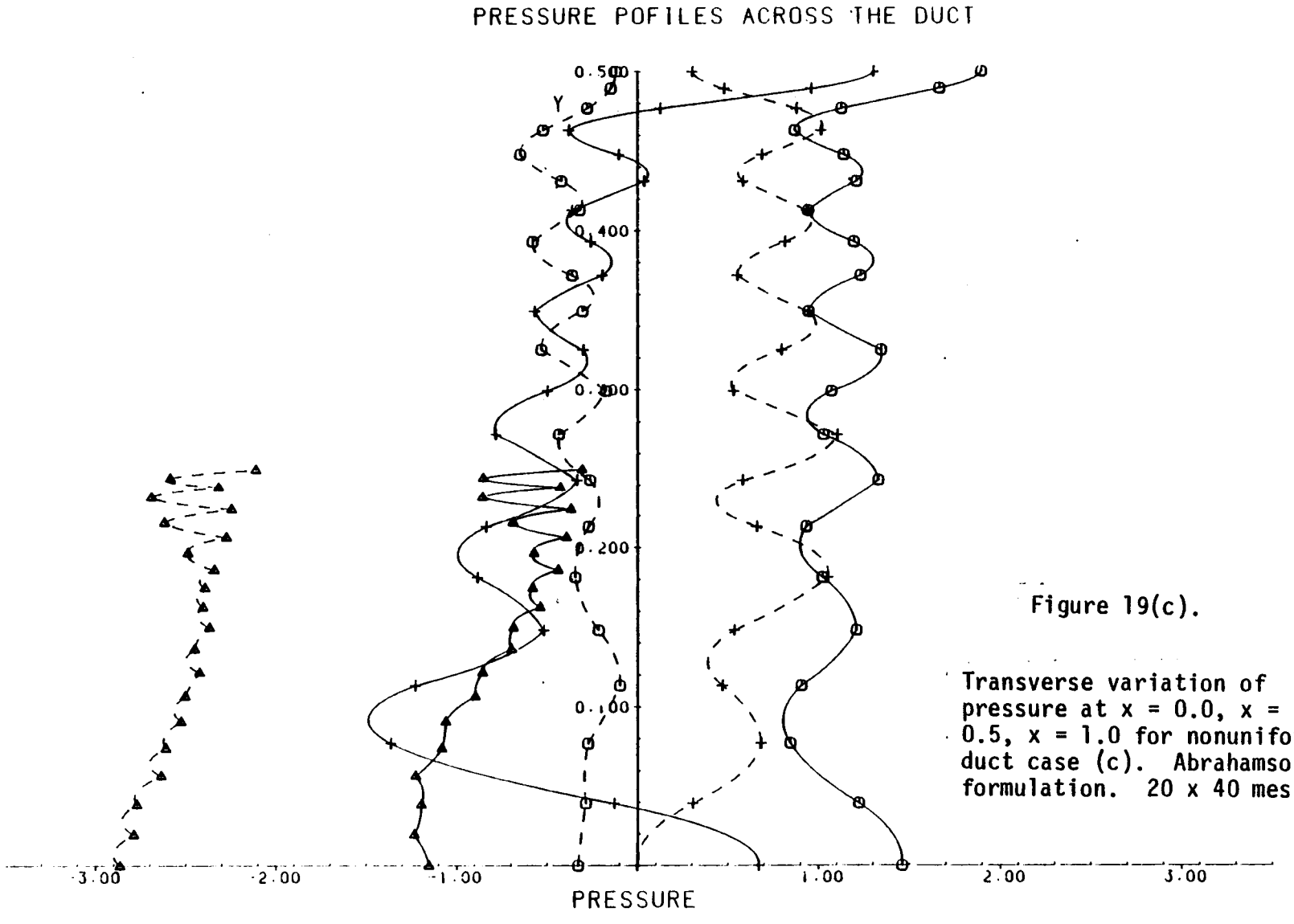

Figure 19(c).

Transverse variation of pressure at x = 0.0, x = 0.5, x = 1.0 for nonuniform duct case (c). Abrahamson formulation. 20 x 40 mesh.

CONCLUSIONS

A combination of analysis and numerical experimentation has been carried out with the goal of examining the convergence characteristics of three finite element algorithms for the modelling of acoustic propagation in nonuniform ducts carrying a mean flow. The first model is based on the assumption of an irrotational mean flow and irrotational acoustic perturbations. This model is currently in use in the calculation of propagation in turbo-fan engine inlets and the subsequent radiation to the far field. In the present study the physical constraints are relaxed to permit a mean flow which is not irrotational, but which is imposed on the irrotational model by entering it as data in the model. As viewed at this point, this is a non-physical model but serves to broaden the scope of the investigation. In the irrotational model the field variables are acoustic velocity potential and acoustic pressure (or density).

The other two models do not impose the irrotational assumption. As a consequence they use the primitive variables, pressure and two components of velocity. One of these models, due to Astley and Eversman [3], takes advantage of natural boundary conditions and introduces the idea of specifying acoustic input, reflection, and transmission boundary conditions in terms of modal amplitudes. The second rotational model is due to Abrahamson [6,7] and uses forced boundary conditions.

In Appendix I it is shown by analysis that under stated restrictions the velocity potential formulation will converge optimally. Numerical experimentation on both uniform and nonuniform duct models verifies the analysis. The stated restrictions are somewhat different than those used in current turbo-fan radiation codes in that (1) velocity potential and pressure are solved for simultaneously (as opposed to solving for potential

and then obtaining pressure by calculation) and (2) the approximation for velocity potential is sought in the subspace of continuous functions while the approximation for pressure is sought in the subspace of discontinuous functions (as opposed to the subspace of continuous functions for both potential and pressure).

No analysis is presently available to isolate the convergence characteristics of either of the two models based on the primitive variables. Information is derived entirely by numerical experimentation. It is found that in the examples considered optimal convergence is not achieved and in some instances lack of convergence is observed. In general, it appears that the Astley-Eversman algorithm displays inconclusive convergence characteristics, certainly not optimal, but not clearly nonconvergent. The Abrahamson algorithm is much more likely to display nonconvergence and this behavior is clearly problem dependent.

It was also noted that the potential formulation, with a rotational mean flow forced on it, does not converge to the same result as the fully rotational models do (when convergence occurs), the difference being more obvious in the boundary layer cases in which a strong shear layer exists. Furthermore, the tendency toward nonconvergence in the rotational models is exacerbated by a strongly sheared boundary layer. The poorest convergence occurred in the numerical experiments using the 1/7 power boundary layer.

It is concluded that:

(1) The potential flow model converges with reasonable assurance.

(2) The rotational flow models are subject to slow convergence or nonconvergence.

(3) Poor convergence or nonconvergence is most likely to occur with strongly sheared flows.

BIBLIOGRAPHY

[1] Tag, I.A. and Akin, J.E., "Finite Element Solution of Sound Propagation in a Variable Area Duct", AIAA-79-0663, 1979.

[2] Eversman, W. and Astley, R. J., "Acoustic Transmission in Non-Uniform Ducts with Mean Flow, Part I: The Method of Weighted Residules", Journal of Sound and Vibration 74(1), p.89-101, 1981.

[3] Astley, R.J. and Eversman, W., "Acoustic Transmission in Non-Uniform Ducts with Mean Flow, Part II: The Finite Element Method", Journal of Sound and Vibration 74(1), p.103-121, 1981.

[4] Baumeister, K.J., "Applications of Velocity Potential Function to Acoustic Duct Propagation and Radiation from Inlets Using Finite Element Theory", AIAA-79-0680, 1979.

[5] Baumeister, K.J., "Time Dependent Difference Theory for Sound Propagation in Axisymmetric Ducts with Plug Flow", AIAA-80-1017, 1980.

[6] Abrahamson, A.L., "ADAM - An Axisymetric Duct Aeroacoustic Modeling System", NASA Contractor Report 3668, 1983.

[7] Abrahamson, A.L., "A Finite Element Algorithm for Sound Propagation in Axisymmetric Ducts Containing Compressible Mean Flow," NASA CR-145209, 1977.

[8] Fix, G.J., Gunzburger, M.D. and Nicolaides, R.A., "On Mixed Finite Element Methods I, The Kelvin Principle", ICASE Report 77-17, December 1977.

[9] Fix, G.J., Gunzburger, M.D. and Nicolaides, R.A., "On Mixed Finite Element Methods II, The Least Squares Method", ICASE Report 77-18, December 1977.

[10] Fix, G.J., Gunzburger, M.D. and Nicolaides, R.A., "On Mixed Finite Element Methods III, The Grid Decomposition Property and Examples", ICASE Report 78-7, March 1978.

[11] Fix, G.J., Gunzburger, M.D., "On Numerical Methods for Acoustic Problems", ICASE Report 78-15, September 1978.

[12] Fix, G.J., Gunzburger, M.D. and Nicolaides, R.A., "On Mixed Finite Element Methods for First Order Elliptic Systems", Numerische Mathematik, 37, p.29-48, 1981.

[13] Fix, G.J., Gunzburger, M.D. and Nicolaides, R.A., "On Finite Element Methods of the Least Squares Type", Computers and Mathematics with Applications, Volume 6, p.87-98, 1979.

[14] Astley, R.J. and Eversman, W., "A Finite Element Formulation of the Eigenvalue Problem in Lined Ducts with Flow", Journal of Sound and Vibration 65(1), p.61-74, 1979.

[15] Ciarlet, P.G., "The Finite Element Method for Elliptic Problems", North Holland, Amsterdam, 1978.

APPENDIX

A FINITE ELEMENT APPROXIMATION OF THE IRROTATIONAL ACOUSTICS EQUATIONS

by

Noel Walkington* and Thomas Wicks†

This work was supported in part by NASA Langley under contract NAG-1-198.

*Department of Mathematics, The University of Texas at Austin, Austin, TX 78712.

†Institute of Applied Mathematics, University of Missouri-Rolla, Rolla, MO 65401.

ABSTRACT

We investigate a finite element approximation of a problem in duct acoustics where the medium is inviscid, the motion is assumed to be irrotational and non-homogeneous boundary conditions are imposed which arise from the approximation of an infinite duct with one that is bounded. A study is made of restrictions for the boundary conditions and their approximation for which a finite element approximation of the mixed-hybrid type is well-posed. In particular we prove that under a reasonable hypothesis on the data that the method will converge optimally if the sequence of boundary coefficients has more than h^{-1} members and the degree of polynomial (k) for the pressure is greater than or equal to the degree, k+1, which is used for the velocity potential.

1. Introduction

The problem of interest is the following: Find $(\phi, p, \{a_n^-\}, \{b_n^+\})$ such that

$$(1.1a) \qquad i\omega c^{-2} p + \underset{\sim}{\nabla} \cdot (\rho \underset{\sim}{\nabla}\phi + c^{-2}\underset{\sim}{U}p) = 0 \quad \text{in} \quad \Omega$$

$$(1.1b) \qquad \rho^{-1} p + \underset{\sim}{U}\cdot\underset{\sim}{\nabla}\phi + i\omega\phi = 0 \quad \text{in} \quad \Omega$$

$$(1.1c) \qquad (\rho \underset{\sim}{\nabla}\phi + c^{-2}\underset{\sim}{U}p)\cdot\underset{\sim}{N}\Big|_{\Gamma_1} = \rho_{\Gamma_1} \sum_{n=0}^{\infty} \delta_n^1 (a_n^+ - a_n^-) \cos(n\pi y/d_1)$$

$$(1.1d) \qquad -(\rho \underset{\sim}{\nabla}\phi + c^{-2}\underset{\sim}{U}p)\cdot\underset{\sim}{N}\Big|_{\Gamma_2} = \rho_{\Gamma_2} \sum_{n=0}^{\infty} \delta_n^2 (b_n^+ - b_n^-) \cos(n\pi y/d_2)$$

$$(1.1e) \qquad \phi|_{\Gamma_1} = \sum_{n=0}^{\infty} (a_n^+ + a_n^-) \cos(n\pi y/d_1)$$

$$(1.1f) \qquad \phi|_{\Gamma_2} = \sum_{n=0}^{\infty} (b_n^+ + b_n^-) \cos(n\pi y/d_2)$$

$$(1.1g) \qquad \frac{\partial\phi}{\partial n} = 0 \quad \text{on} \quad \Gamma_3 \cup \Gamma_4$$

$\Omega \subset \mathbb{R}^2$ represents a duct with boundary $\partial\Omega = \bigcup_{i=1}^{4} \Gamma_i$ where $\Gamma_1 = \{(0,y): y \in]0,d_1[\}$ and $\Gamma_2 = \{(L,y): y \in]0,d_2[\}$. In addition Γ_3 and Γ_4 are assumed to be such that Ω satisfies the cone condition. The variables of interest $p(\underset{\sim}{x})$, $\phi(\underset{\sim}{x}) \in \mathbb{C}$ define the acoustic pressure and velocity potential; $\underset{\sim}{U} \in L^{\infty}(\bar{\Omega})^2$ represents the mean velocity; $c, \rho \in L^{\infty}(\bar{\Omega})$ denote the sound speed and gas density; ω denotes the pertubation frequency; and $\{a_n^+\} = \{a_n^+\}_{n=0}^{\infty}$ and $\{b_n^-\} = \{b_n^-\}_{n=0}^{\infty}$ represent incoming waves and are assumed to be known. Also,

$$\delta_n^i = i[k_{\Gamma_i}^2 - (1-M_{\Gamma_i}^2)(n\pi/d_i)^2]^{\frac{1}{2}} \; ; \; i = 1,2$$

where $M = |\underset{\sim}{U}|/c$ and $k = \omega/c$ represent the mach number and characteristic wavelength respectively and M_{Γ_i}, etc. denotes its restriction to Γ_i, i=1 or 2.

Equations (1.1a-b) are a model for an inviscid, non-heat conducting, ideal fluid which is undergoing an irrotational, "small", periodic-pertubation about a subsonic mean flow ($M < 1$) in a duct. The boundary conditions (1.1c-d) define compatibility conditions between incident and reflected waves in a uniform duct (cf. Eversman and Astley [3]).

The compressible flow equations have received considerable, attention in the literature (e.g. Bristeau et al. [1]) and equations (1.1a-b) represent a linearization of these. Also Fix and Nicolaides [4] have studied a mixed model with Dirichlet boundary conditions for the case when the flow is possibly rotational but $\underset{\sim}{U} = \underset{\sim}{0}$ (i.e. a mixed model for Helmholtz's equation). In particular they have investigated conditions under which an increased convergence rate holds for the pressure (see also Fix et al. [5] and Fix and Gunzburger [6]).

We will study a finite element approximation to (1.1) which is mixed in the sense that (ϕ,p) are approximated independently and hybrid in the sense that $(\phi,\{a_n^-\},\{b_n^+\})$ are approximated independently. In section 2 we define a weak problem for the boundary-value problem and specify a finite element approximation. Then in section 3 we prove that the weak problem is well-posed and in section 4 we prove that the finite element approximation converges under suitable hypotheses.

2. The Finite Element Approximation

We first define a weak problem which is associated with (1.1) and then consider a finite element approximation of this problem. First we fix some notation.

Let $H^s(\Omega)$, $\infty > s \geq 0$, denote the usual Sobolev space over the complex field and define $S = \{ \{g_n\}_{n=0}^{\infty} \in \ell^2(\mathbb{N}\cup\{0\}): \sum_{n=1}^{\infty} n|g_n|^2 + |g_0|^2 < \infty\}$ where $\ell^2(\mathbb{N}\cup\{0\})$ denotes the space of square-summable sequences of complex numbers. In addition $\|\cdot\|_{s,\Omega}$ and $\|\cdot\|_S$ will denote the usual norms for $H^s(\Omega)$ and S respectively. Also set $\Gamma_5 \subset \Gamma_4$ with meas $\Gamma_5 > 0$, let $H = \{g \in H^1(\Omega): g|_{\Gamma_5} = 0\}$ and define,

$$\hat{n}(n) = \begin{cases} 1 & n = 0 \\ n & n \in \mathbb{N} \end{cases}$$

$$B_n^i(g_n,\psi) = g_n \int_{\Gamma_i} \bar{\psi}(y) \cos(n\pi y/d_i)dy \quad \forall \{g_n\} \in S,\ \psi \in H\ ;\ i = 1,2$$

Weak Problem: Find $(\phi,p,\{a_n^-\},\{b_n^+\}) \in H \times L^2(\Omega) \times S \times S$ such that,

$$(2.1a) \quad \int_{\Omega} [- i\omega c^{-2} p\bar{\psi} + (\rho\nabla\phi + c^{-2}\underset{\sim}{U}\, p) \cdot \nabla\bar{\psi}]$$

$$+ \rho_{\Gamma_1} \sum_{n=0}^{\infty} \delta_n^1 B_n^1(a_n^-,\psi) + \rho_{\Gamma_2} \sum_{n=0}^{\infty} \delta_n^2 B_n^2(b_n^+,\psi)$$

$$= \rho_{\Gamma_1} \sum_{n=0}^{\infty} \delta_n^1 B_n^1(a_n^+,\psi) + \rho_{\Gamma_2} \sum_{n=0}^{\infty} \delta_n^2 B_n^2(b_n^-,\psi)$$

$$(2.1b) \quad \int_{\Omega} [\rho^{-1}p + \underset{\sim}{U}.\nabla\phi + i\omega\phi]\, \bar{q} = 0$$

$$(2.1c)\qquad \sum_{n=0}^{\infty} \hat{n}(n)(a_n^- + a_n^+)\bar{\alpha}_n = (2/d_1) \sum_{n=1}^{\infty} n\, B_n^1(\bar{\alpha}_n, \bar{\phi}) + d_1^{-1} B_0^1(\bar{\alpha}_0, \bar{\phi})$$

$$(2.1d)\qquad \sum_{n=0}^{\infty} \hat{n}(n)(b_n^+ + b_n^-)\,\bar{\beta}_n = (2/d_2) \sum_{n=1}^{\infty} n\, B_n^2(\bar{\beta}_n, \bar{\phi}) + d_2^{-1} B_0^2(\bar{\beta}_0, \bar{\phi})$$

$$\forall\, (\psi, q, \{\alpha_n\}, \{\beta_n\}) \in H \times L^2(\Omega) \times S \times S$$

Remark 2.1. The requirement that $\phi = 0$ on Γ_5 is a technical detail which is dependent on the specific choice of data. For convenience we will always include this condition.

Remark 2.2. A weak problem with fewer unknown variables may be constructed by eliminating the pressure, $\{a_n^-\}$ and $\{b_n^+\}$. However these variables are required by Acousticians for comparisons with experiments.

In constructing the finite element approximation we shall need the following standard notions (cf. Ciarlet [2]). Let $\mathcal{T}_h$ denote a regular family of triangulations of Ω where h denotes the maximum diameter of the element partition. Define

$$\mathbb{P}_k(T) = \{\text{polynomials of degree} \le k \text{ on } T\},\ T \in \mathcal{T}_h$$

$$\mathbb{M}_k(\mathcal{T}_h) = \{g \in C(\Omega):\ g|_{\Gamma_5} = 0,\ g|_T = f + i\hat{f} \text{ where } f,\ \hat{f} \in \mathbb{P}_k(T)$$

$$\forall\, T \in \mathcal{T}_h\},\ k \ge 1$$

$$\mathbb{M}_k^{-1}(\mathcal{T}_h) = \{g \in L^2(\Omega):\ g|_T = f + i\hat{f} \text{ where } f,\ \hat{f} \in \mathbb{P}_k(T)$$

$$\forall\, T \in \mathcal{T}_h\},\ k \ge 0$$

$$S_N = \{\, \{g_n\}_{n=0}^{N} \subset \mathbb{C}:\ \sum_{n=1}^{N} n|g_n|^2 + |g_0|^2 < \infty\},\ N \ge 0$$

Here $C(\Omega)$ denotes the complex-valued functions which are continuous.

Approximation: Find $(\phi_h, p_h, \{a_n^{-N}\}, \{b_n^{+N}\}) \in \mathbb{M}_\ell(T_h) \times \mathbb{M}_m^{-1}(T_h) \times S_N \times S_N$ such that,

$$(2.2a) \quad \int_\Omega [- i\omega c^{-2} p_h \bar{\psi}_h + (\rho \nabla \phi_h + c^{-2} \underset{\sim}{U} p_h) \cdot \nabla \bar{\psi}_h]$$

$$+ \rho_{\Gamma_1} \sum_{n=0}^{N} \delta_2^1 B_n^1(a_n^{-N}, \psi_h) + \rho_{\Gamma_2} \sum_{n=0}^{N} \delta_n^2 B_n^2(b_n^{+N}, \psi_h)$$

$$= \rho_{\Gamma_1} \sum_{n=0}^{N} \delta_n^1 B_n^1(a_n^{+}, \psi_h) + \rho_{\Gamma_2} \sum_{n=0}^{N} \delta_n^2 B_n^2(b_n^{-}, \psi_h)$$

$$(2.2b) \quad \int_\Omega [\rho^{-1} p_h + \underset{\sim}{U} \cdot \nabla \phi + i\omega \phi_h] \bar{q}_h = 0$$

$$(2.2c) \quad \sum_{n=0}^{N} \hat{n}(n)(a_n^{-N} + a_n^{+}) \bar{\alpha}_n^N = (2/d_1) \sum_{n=1}^{N} n B_n^1(\bar{\alpha}_n^N, \bar{\phi}_h) + d_1^{-1} B_0^1(\bar{\alpha}_0^N, \bar{\phi}_h)$$

$$(2.2d) \quad \sum_{n=0}^{N} \hat{n}(n)(b_n^{+N} + b_n^{-}) \bar{\beta}_n^N = (2/d_2) \sum_{n=1}^{N} n B_n^2(\bar{\beta}_n^N, \bar{\phi}_h^N) + d_2^{-1} B_0^2(\bar{\beta}_0^N, \bar{\phi}_h)$$

$$\forall (\psi_h, q_h, \{\alpha_n^N\}, \{\beta_n^N\}) \in \mathbb{M}_\ell(T_h) \times \mathbb{M}_m^{-1}(T_h) \times S_N \times S_N$$

where $\ell \geq 1$, $m \geq 0$ and $N \geq 0$

2.1 Preliminaries

Set $\| \cdot \|_0 = \| \cdot \|_{0,\Omega}$ and $\| \cdot \|_1 = \| \cdot \|_{1,\Omega}$. We will list some lemmas and hypotheses that will be needed in the sequel. First the standard Poincaré inequality.

Lemma 2.1. Suppose Ω satisfies the cone condition and meas $\Gamma_5 > 0$. Then there exists a $\lambda > 0$ such that

$$\|\nabla\phi\|_0^2 \geq \lambda \|\phi\|_0^2 \qquad \forall \phi \in H$$

Lemma 2.2. Let $\{\alpha_n\} \in S$, $\psi \in H$ and suppose Ω satisfies the cone condition. Then for i=1,2 there exists a positive constant $\gamma(d_i)$ such that

$$\sum_{n=0}^{\infty} \hat{n}(n) |B_n^i(\alpha_n,\psi)| \leq \gamma d_i^{\frac{1}{2}} \max\,(1,(d_i/\pi)^{\frac{1}{2}}) \| \{\alpha_n\} \|_S \| \psi \|_1$$

Proof. First note that by the trace theorem, Lions and Magenes [7], there exists a $\gamma > 0$ such that $\forall \psi \in H$, $\psi|_{\Gamma_i} \in H^{\frac{1}{2}}(\Gamma_i)$, and $\| \psi \|_{\frac{1}{2},\Gamma_i} \leq \gamma \| \psi \|_1$ for i = 1,2 since $\Gamma_i \subset \partial\Omega$. Then because of the definition of $B_n^i(\cdot,\cdot)$ and the Cauchy-Schwarz inequality, $B_n^i(\alpha_n,\psi)$ exists and

$$\sum_{n=0}^{\infty} \hat{n}(n) |B_n^i(\alpha_n,\psi)| \leq d_i^{\frac{1}{2}} \| \{\alpha_n\} \|_S \| \{\psi_n^i\} \|_S$$

where $\psi_n^i = \int_{\Gamma_i} \psi e_n^i$ with $\{e_n^i\}$ being defined by

$$e_n^i(y) = \begin{cases} d_i^{-\frac{1}{2}} & n=0 \\ (2/d_i)^{\frac{1}{2}} \cos\,(n\pi y/d_i) & n \in \mathbb{N} \end{cases}$$

Now by using classical interpolation theory for Sobolev spaces (cf. Lions and Magenes [7]) $H^{\frac{1}{2}}(\Gamma_i) = \{g: g \in \mathrm{Dom}([I-D^2]^{\frac{1}{4}})\}$ may be constructed as an intermediate space between $L^2(\Gamma_i)$ and $\{g \in H^1(\Gamma_i): Dg(0) = Dg(d_i) = 0\}$. Hence

$$\| \psi \|^2_{\frac{1}{2},\Gamma_i} = \sum_{n=0}^{\infty} [1 + (n\pi/d_i)^2]^{\frac{1}{2}} |\psi_n^i|^2 \geq \min(1,\pi/d_i) \| \{\psi_n^i\} \|^2_S$$

which leads to the desired estimate after we combine inequalities.

Next we cite a standard result of approximation theory (cf. Ciarlet [2]). Let $| \cdot |_{m,\Omega}$, for $m \in \mathbb{N}$, denote the usual seminorm on $H^m(\Omega)$.

Lemma 2.3. Suppose $\psi \in H^{k+1}(\Omega)$, $k \geq 1$, and $q \in H^{m+1}(\Omega)$, $m \geq 0$. Then if $\mathcal{T}_h$ is a regular family of triangulations of Ω, there exists a C_1, $C_2 > 0$ (independent of h, ψ and q) such that

$$\inf_{v_h \in \mathbb{M}_k(\mathcal{T}_h)} \| \psi - v_h \|_1 \leq C_1 h^k |\psi|_{k+1,\Omega}$$

$$\inf_{v_h \in \mathbb{M}_m^{-1}(\mathcal{T}_h)} \| q - v_h \|_0 \leq C_2 h^{m+1} |q|_{m+1,\Omega}$$

We now list some reasonable hypotheses that the known variables should satisfy.

Hypothesis 2.1. $\{a_n^+\}$, $\{b_n^-\} \in S$; $c, \rho \in L^\infty(\overline{\Omega})$; $\omega \in \{g \in \mathbb{R}: g \geq 0\}$; and $\underset{\sim}{U} \in L^\infty(\overline{\Omega})^2$ with

$$\operatorname{ess\,inf}_{\underset{\sim}{x} \in \overline{\Omega}} c(\underset{\sim}{x}) = c_0 > 0$$

$$\| c \|_{L^\infty(\Omega)} = c_1$$

$$\operatorname{ess\,inf}_{\underset{\sim}{x} \in \overline{\Omega}} \rho(\underset{\sim}{x}) = \rho_0 > 0$$

$$\| \rho \|_{L^\infty(\overline{\Omega})} = \rho_1$$

$$\| \underset{\sim}{U} \|_{L^\infty(\overline{\Omega})^2} = U_1$$

Here $L^\infty(\Omega)^N$, for $N = 1,2$ is defined on the real scalars.

We close with a standard approximation result for sequences. First we define for $r \geq 0$

$$S^r = \{\{g_n\} \in \ell^2(\mathbb{N} \cup \{0\}): \sum_{n=0}^{\infty} \hat{n}(n)^{2r+1} |g_n|^2 < \infty\}$$

Lemma 2.4. Let $\{\alpha_n\} \in S^r$, $r \geq 0$. Then for $N \geq 0$ there exists a positive scalar C such that

$$\inf_{\{g_n\} \in S_N} \|\{\alpha_n - g_n\}\|_S \leq C N^{-r} \|\{\alpha_n\}\|_{S^r}$$

3. Existence and Uniqueness of Solutions

We note that the form on $(H \times L^2(\Omega) \times S \times S)^2$, which represents the left hand side of (2.1a-b) and the right hand side of (2.1c-d), is sesquilinear and the form on $H \times L^2(\Omega) \times S \times S$, which represents the right hand side of (2.1a-b) and the left hand side of (2.1c-d), is antilinear. Thus to prove that the weak problem has a unique solution it suffices to show that the conditions of the Lax-Milgram theorem are satisfied.

First observe that from the definition of δ_n^i, along with Hypothesis 2.1, that

$$(3.1) \qquad |\delta_n^i| \leq k_i \hat{n}(n) \qquad \text{for } i = 1,2$$

where $k_i = [k_{\Gamma_i}^2 + |1 - M_{\Gamma_i}^2|(\pi/d_i)^2]^{\frac{1}{2}}$; let $u = (\phi, p, \{a_n^-\}, \{b_n^+\})$, $v = (\psi, q, \{\alpha_n\}, \{\beta_n\})$, $U = H \times L^2(\Omega) \times S \times S$, $\|u\|_U^2 = \|\phi\|_1^2 + \|p\|_0^2 + \|\{a_n^-\}\|_S^2 + \|\{b_n^+\}\|_S^2$ $\forall u \in U$; and define

$$F(v) = \rho_{\Gamma_1} \sum_{n=0}^{\infty} \delta_n^1 B_n^1(a_n^+, \psi) + \rho_{\Gamma_2} \sum_{n=0}^{\infty} \delta_n^2 B_n^2(b_n^-, \psi)$$

$$- \sum_{n=0}^{\infty} \hat{n}(n)(a_n^+ \bar{\alpha}_n + b_n^- \bar{\beta}_n)$$

$$A(u,v) = \int_\Omega [- i\omega c^{-2} p\bar{\psi} + (\rho \nabla\phi + c^{-2} \underset{\sim}{U} p) \cdot \nabla\bar{\psi} + \rho^{-1} p\bar{q}$$

$$+ (\underset{\sim}{U} \cdot \nabla\phi)\bar{q} + i\omega\phi\bar{q} - (2/d_1) \sum_{n=1}^{\infty} n B_n^1(\bar{\alpha}_n, \bar{\phi}) + \sum_{n=0}^{\infty} \hat{n}(n) a_n^- \bar{\alpha}_n$$

$$- d_1^{-1} B_0^1(\bar{\alpha}_0, \bar{\phi}) - (2/d_2) \sum_{n=1}^{\infty} n B_n^2(\bar{\beta}_n, \bar{\phi}) + \sum_{n=0}^{\infty} \hat{n}(n) b_n^+ \bar{\beta}_n$$

$$- d_2^{-1} B_0^2(\bar{\beta}_0, \bar{\phi}) + \sum_{n=0}^{\infty} [\rho_{\Gamma_1} \delta_n^1 B_n^1(a_n^-, \psi_h) + \rho_{\Gamma_2} \delta_n^2 B_n^2(b_n^+, \psi_h)]$$

Lemma 3.1. Suppose Hypothesis 2.1 holds and Ω satisfies the cone condition. Then $F \in U'$ and A is a continuous sesquilinear form on $U \times U$.

Proof. From the definition of F, use of the Cauchy-Schwarz inequality, Hypothesis 2.1, 3.1 , and Lemma 2.2 we have that

$$|F(v)| \leq \rho_{\Gamma_1} k_1 \gamma d_1^{\frac{1}{2}} \max\,(1,(d_1/\pi)^{\frac{1}{2}}) \|\{a_n^+\}\|_S \|\psi\|_1$$

$$+ \rho_{\Gamma_2} k_2 \gamma d_2^{\frac{1}{2}} \max\,(1,(d_2/\pi)^{\frac{1}{2}}) \|\{b_n^-\}\|_S \|\psi\|_1$$

$$+ \|\{a_n^+\}\|_S \|\{\alpha_n\}\|_S + \|\{b_n^-\}\|_S \|\{\beta_n\}\|_S$$

thus

$$\|F\|_{U'} \leq \max\left(1, \max_{i=1,2}[\rho_\Gamma d_i^{\frac{1}{2}} k_i \max\,(1,(d_i/\pi)^{\frac{1}{2}})\gamma]\right)(\|\{a_n^+\}\|_S + \|\{b_n^-\}\|_S)$$

hence $F \in U'$. Now if we perform similar operations on $A(\cdot,\cdot)$

$$|A(u,v)| \leq \max\Big(\omega c_0^{-2},\ \rho_1,\ U_1 c_0^{-2},\ \rho_0^{-1},\ U_1,\ \omega, 1,$$

$$\max_{i=1,2}\,[(\rho_{\Gamma_i} k_i d_i^{\frac{1}{2}} + 2d_i^{-\frac{1}{2}})\ \max(1,(d_i/\pi)^{\frac{1}{2}})]\gamma\Big)\|u\|_U \|v\|_U$$

which completes the proof.

Define $\xi_1 = \gamma \max_{i=1,2}\,[(2 + \rho_{\Gamma_i} k_i d_i) d_i^{-\frac{1}{2}} \max\,(1,(d_i/\pi)^{\frac{1}{2}})]$ and $\xi_2 = (U_1 + \omega/\sqrt{\lambda})(1+c_0^{-2})$.

Theorem 3.1. Suppose Hypothesis 2.1 holds and Ω satisfies the cone condition. Then if there exists a positive number ε such that

$$2\,\xi_1 < 8\,\varepsilon < (4\rho_0\lambda/(1+\lambda) - \xi_2^2\rho_1)/\xi_1$$

there exists a unique $u \in U$ satisfying (2.1) with $\|u\|_U \leq C\ (\|\{a_n^+\}\|_S + \|\{b_n^-\}\|_S)$ where $C > 0$.

Proof. Lemma 3.1 holds therefore we need only prove that A is coercive on $U \times U$. Using Lemmas 2.1 and 2.2, Hypothesis 2.1 and the Cauchy-Schwarz inequality,

$$\text{Re } A(u,u) \geq \rho_0\lambda/(1+\lambda)\,\|\phi\|_1^2 + \rho_1^{-1}\|p\|_0^2 + \|\{a_n^-\}\|_S^2 + \|\{b_n^+\}\|_S^2$$

$$- \xi_2\,\|p\|_0\,\|\phi\|_1 - \xi_1\|\phi\|_1(\|\{a_n^-\}\|_S + \|\{b_n^+\}\|_S)$$

and by applying the arithmetic-geometric mean inequality to the last two terms we have with $C_1 = \rho_0\lambda/(1+\lambda) - \xi_2\hat{\epsilon} - 2\xi_1\epsilon$, $C_2 = 1/\rho_1 - \xi_2/4\hat{\epsilon}$ and $C_3 = 1 - \xi_1/4\epsilon$:

$$\text{Re } A(u,u) \geq C_1\,\|\phi\|_1^2 + C_2\,\|p\|_0^2 + C_3(\|\{a_n^-\}\|_S^2 + \|\{b_n^+\}\|_S^2)$$

Now $\hat{\epsilon} > 0$ may be chosen so that

$$C_1 = C_2 = \rho_0\lambda/(1+\lambda) - [C_4 + (C_4^2 + \xi_2^2)^{1/2}]/2 - 2\xi_1\epsilon$$

where $C_4 = \rho_0\lambda/(1+\lambda) - 1/\rho_1 - 2\xi_1\epsilon$. Thus by hypothesis (after some manipulation) $C_1, C_3 > 0$. Hence A is coercive on $U \times U$ and the Lax-Milgram theorem holds therefore completing the proof.

Theorem 3.1 may also be extended to apply to the approximation. First note that $\mathbb{M}_\ell(T_h)$ with $\|\cdot\|_1$ and $\mathbb{M}_m^{-1}(T_h)$ with $\|\cdot\|_0$ are closed subspaces of H and $L^2(\Omega)$. Furthermore if we extend $\{g_n^N\} \in S_N$ to $\{g_n^N\} \in S$ by defining $g_n^N = 0 \quad \forall\ n > N$ then S_N with $\|\cdot\|_S$ is a closed subspace of S. Thus by repeating the proof for the finite dimensional case we have:

Theorem 3.2. Suppose the hypothesis of Theorem 3.1 holds. Then there exist a unique $u_h = (\phi_h, p_h, \{a_n^{-N}\}, \{b_n^{+N}\}) \in U_h = \mathbb{M}_\ell(T_h) \times \mathbb{M}_m^{-1}(T_h) \times S_N \times S_N$ satisfying (2.2) with $\|u_h\|_U \leq C\,(\|\{a_n^+\}\|_S + \|\{b_n^-\}\|_S)$.

4. Convergence of the Approximation

We now prove convergence of the approximation (2.2) to the solution of (2.1) under an hypothesis that the solution and the data is "regular".

Set $v_h = (\psi_h, q_h, \{\alpha_n^N\}, \{\beta_n^N\}) \in U_h$ and define

$$F_N(v_h) = \rho_{\Gamma_1} \sum_{n=0}^{N} \delta_n^1 B_n^1(a_n^+, \psi_h) + \rho_{\Gamma_2} \sum_{n=0}^{N} \delta_n^2 B_n^2(b_n^-, \psi_h)$$

$$- \sum_{n=0}^{N} \hat{n}(n) (a_n^+ \bar{\alpha}_n^N + b_n^- \bar{\beta}_n^N)$$

$$A_N(u_h, v_h) = \int_\Omega [- i\omega c^{-2} p_h \bar{\psi}_h + (\rho \nabla \phi_h + c^{-2} \underset{\sim}{U} p) \cdot \nabla \bar{\psi} + p^{-1} p_h \bar{q}_h$$

$$+ (\underset{\sim}{U} \cdot \nabla \phi_h) \bar{q}_h + i\omega \phi_h \bar{q}_h] - (2/d_1) \sum_{n=1}^{N} n B_n^1(\bar{\alpha}_n^N, \bar{\phi}_h) + \sum_{n=0}^{N} \hat{n}(n) a_n^{-N} \bar{\alpha}_n^N$$

$$- d_1^{-1} B_0^1(\bar{\alpha}_0^N, \bar{\phi}_h) - (2/d_2) \sum_{n=1}^{N} n B_n^2(\bar{\beta}_n^N, \bar{\phi}_h) + \sum_{n=0}^{N} n(n) b_n^{+N} \bar{\beta}_n^N$$

$$- d_2^{-1} B_0^2(\bar{\beta}_0^N, \bar{\phi}_h) + \sum_{n=0}^{N} [\rho_{\Gamma_1} \delta_n^1 B_n^1(a_n^{-N}, \psi_h) + \rho_{\Gamma_2} \delta_n^2 B_n^2(b_n^{+N}, \psi_h)]$$

Theorem 4.1. Suppose the hypothesis of Theorem 3.1 holds, T_h is a regular family of triangulations, $\ell \geq 1$, $m \geq 0$, $r > 0$, u and u_h are solutions to (2.1) and (2.2) with $u \in (H \cap H^{\ell+1}(\Omega)) \times H^{m+1}(\Omega) \times S^r \times S^r$ and $\{a_n^+\}, \{b_n^-\} \in S^r$. Then there exists a positive constant C such that,

$$\| u - u_h \|_U \leq C[h^\ell |\phi|_{\ell+1,\Omega} + h^{m+1} |p|_{m+1,\Omega} + N^{-r}(\|\{a_n^+\}\|_{S^r}$$

$$+ \|\{a_n^-\}\|_{S^r} + \|\{b_n^+\}\|_{S^r} + \|\{b_n^-\}\|_{S^r})]$$

Proof. Let $e = u - u_h$. Then $A(e,e) = A(e,u-v_h) + A(e,v_h-u_h)$ $\forall$ $v_h \in U_h$ since A is sesquilinear. But A is continuous and coercive on $U \times U$ (and $U_h \times U_h$); u and u_h are solutions to (2.1) and (2.2); and $A_N(u_h,v_h) = A(u_h,v_h)$. Thus

$$\| u - u_h \|_U \leq C[\| u - v_h \|_U + |F(u_h-v_h) - F_N(u_h - v_h)|/\| u - u_h \|_U]$$

Now

$$F(v_h) - F_N(v_h) = \sum_{n=N+1}^{\infty} [\rho_{\Gamma_1} \delta_n^1 B_n^1(a_n^+,\psi_h) + \rho_{\Gamma_2} \delta_n^2 B_n^2(b_n^-,\psi_h)]$$

Therefore by using (3.1), noting that $\forall \{g_n\} \in S^r$ and $i = 1,2$

$$\sum_{n=N+1}^{\infty} \hat{n}(n)|B_n^i(g_n,\psi_h)| \leq N^{-r} \sum_{n=0}^{\infty} \hat{n}(n) |B_n^i(\hat{n}(n)^r g_n,\psi_h)|$$

and applying Lemma 2.2 we get that

$$|F(v_h) - F_N(v_h)| \leq \xi_1 N^{-r} \| \psi_h \|_1 (\|\{a_n^+\}\|_{S^r} + \|\{b_n^-\}\|_{S^r})$$

We obtain the desired result after choosing v_h so that Lemmas 2.3 and 2.4 hold.

As might be expected we may not approximate (2.1) with arbitrary values for ℓ, m and N without possibly sacrificing accuracy. A judicious choice may be realized by observation of the estimate $\| u - u_h \|_U$.

Corollary 4.1. Suppose that $m \geq \ell-1$ and $N \geq h^{-\ell/r}$. Then

$$\| u - u_h \|_U = O(h^{\ell})$$

Remark 4.1. Corollary 4.1 allows one to determine how many boundary terms must be included in the approximation depending on the regularity of the boundary data. In many acoustics problems we find that $N = 1$ implying that $N \geq (1/h)$.

4.1 Numerical Example

We consider a problem which is not explicitly covered by our theory but nevertheless can be analyzed in a similar manner. Let $\Omega = \{(x,y): 0 < x < 1,\ 0 < y < 0.5\}$, $c(x,y) = 1.\ \forall\ (x,y) \in \overline{\Omega}$ and define for $0 \leq y \leq 0.5$

$$\rho(x,y) = \begin{cases} 1. & 0 \leq x < 0.5 \\ 0.5 & 0.5 \leq x \leq 1. \end{cases}$$

Also let $\underset{\sim}{e}_x$ define a unit vector in the x-direction, set

$$\underset{\sim}{U} = \begin{cases} -0.25\ \underset{\sim}{e}_x & 0 \leq x < 0.5 \\ -0.5\ \underset{\sim}{e}_x & 0.5 \leq x \leq 1. \end{cases}$$

$\omega = 1.$, $a_0^+ = 1.$, $a_n^+ = 0.\ \forall\ n \geq 1$, $b_n^- = 0\ \forall\ n \geq 0$ and append to (1.1) the following jump condition for $\hat{x} = 0.5$, $0 < y < 0.5$.

$$\lim_{\varepsilon \to 0} \left([\rho(\hat{x}-\varepsilon,y)\underset{\sim}{\nabla}\phi(\hat{x}-\varepsilon,y) + c^{-2}p(\hat{x}-\varepsilon,y)\underset{\sim}{U}(\hat{x}-\varepsilon,y)] \cdot \underset{\sim}{e}_x \right)$$

$$= \lim_{\varepsilon \to 0} \left([\rho(\hat{x}+\varepsilon,y)\underset{\sim}{\nabla}\phi(\hat{x}+\varepsilon,y) + c^{-2}p(\hat{x}+\varepsilon,y)\underset{\sim}{U}(\hat{x}+\varepsilon,y)] \cdot \underset{\sim}{e}_x \right)$$

We then have a classical problem which has as a solution for ϕ, $\{a_n^-\}$ and $\{b_n^+\}$:

$$\phi(x,y) = \begin{cases} \exp(-4/3\ i x) + a_0^- \exp(4/5\ i x), & 0 < x < 0.5 \\ b_0^+ \exp(-2\ i[x-1]), & 0.5 < x < 1. \end{cases}$$

$$a_0^- \simeq 0.161 - 0.219\ i\ ;\ a_n^- = 0 \quad \forall\ n \in \mathbb{N}$$

$$b_0^+ \simeq -0.1276 - 1.3272\ i\ ;\ b_n^+ = 0 \quad \forall\ n \in \mathbb{N}$$

The pressure may be calculated using (1.1b) and the jump condition.

Remark 4.3. This solution does not satisfy the hypothesis of Theorem 4.1. However the same convergence rates will hold for our approximation as long as the graph $\{(0.5,y): 0 \leq y \leq 0.5\}$ does not intersect the interior of any element in T_h. Otherwise, as is well known, we would have to use discontinuous interpolating functions for the approximation.

Three numerical experiments were performed using uniform rectangular elements. We denote a uniform grid with I elements in the x direction and J elements in the y direction as a "J x I grid".

The three cases we consider are:

(1) $(\phi_h,p_h) \in M_2 \times M_1^{-1}$ with 5 x 10, 10 x 20 and 20 x 40 grids.

(2) $(\phi_h,p_h) \in M_2 \times M_1^{-1}$ with 5 x 10, 10 x 21 and 20 x 41 grids.

(3) $(\phi_h,p_h) \in M_2 \times M_1$ with 5 x 10, 10 x 20 and 20 x 40 grids.

The error in pressure is tabulated in Table 1 for each of the experiments. Experiment 1 yielded the desired convergence rate (rate $\approx$ 2) while the other two experiments did not (rate $\approx$ 1) as expected.

References

[1] M. O. Bristeau, R. Glowinski, J. Periaux, P. Perrier, O. Pironneau and G. Poirier, Transonic flow simulations by finite elements and least square methods, Proceedings of the Third International Conference on Finite Elements in Flow Problems, Banff, Alberta, Canada, 1980, pp. 11-29.

[2] P. G. Ciarlet, The Finite Element Method for Elliptic Problems, North-Holland, Amsterdam, 1978.

[3] W. Eversman and R. J. Astley, Acoustic transmission in non-uniform ducts with mean flow; Part 1: The method of weighted residuals, J. Sound Vib., 74 (1981), pp. 89-101.

[4] G. J. Fix and R. A. Nicolaides, An analysis of mixed finite element approximations for periodic acoustic wave propagation, SIAM J. Numer. Anal., 17 (1980), pp. 779-786.

[5] G. J. Fix, M. D. Gunzburger and R. A. Nicolaides, On finite element methods of the least squares type, Comp. & Maths. with Appls., 5 (1979), pp. 87-98.

[6] G. J. Fix and M. D. Gunzburger, On numerical methods for acoustic problems, Comp. & Maths. with Appls., 6 (1980), pp. 265-278.

[7] J. L. Lions and E. Magenes, Non-Homogeneous Boundary-Value Problems and Applications, Springer, Berlin, 1972.

Experiment 1			Experiment 2			Experiment 3		
Mesh (N)	$\|\| p_h \|\|_0$	$\|\| p - p_h \|\|_0$	Mesh (N)	$\|\| p_h \|\|_0$	$\|\| p - p_h \|\|_0$	Mesh (N)	$\|\| p_h \|\|_0$	$\|\| p - p_h \|\|_0$
5 x 10 (5)	1.0260	1.098×10^{-3}	5 x 11 (5)	1.0226	1.812×10^{-2}	5 x 10 (5)	1.0247	2.308×10^{-2}
10 x 20 (5)	1.0260	2.746×10^{-4}	10 x 21 (5)	1.0242	1.292×10^{-2}	10 x 20 (5)	1.0253	1.641×10^{-2}
20 x 40 (10)	1.0260	6.865×10^{-5}	20 x 41 (10)	1.0250	9.171×10^{-3}	20 x 40 (10)	1.0256	1.162×10^{-2}

TABLE 1. NUMERICAL RESULTS